



# Targeted glycan degradation potentiates the anticancer immune response in vivo

Melissa A. Gray<sup>1</sup>, Michal A. Stanczak<sup>2,3</sup>, Natália R. Mantuano<sup>2,3</sup>, Han Xiao<sup>1</sup>, Johan F. A. Pijnenborg<sup>1</sup>, Stacy A. Malaker<sup>1</sup>, Caitlyn L. Miller<sup>4</sup>, Payton A. Weidenbacher<sup>1</sup>, Julia T. Tanzo<sup>1</sup>, Green Ahn<sup>1</sup>, Elliot C. Woods<sup>1</sup>, Heinz Läubli<sup>2,3</sup> and Carolyn R. Bertozzi<sup>1,5</sup> ✉

**Currently approved immune checkpoint inhibitor therapies targeting the PD-1 and CTLA-4 receptor pathways are powerful treatment options for certain cancers; however, most patients across cancer types still fail to respond. Consequently, there is interest in discovering and blocking alternative pathways that mediate immune suppression. One such mechanism is an upregulation of sialoglycans in malignancy, which has been recently shown to inhibit immune cell activation through multiple mechanisms and therefore represents a targetable glycoimmune checkpoint. Since these glycans are not canonically druggable, we designed an  $\alpha$ HER2 antibody-sialidase conjugate that potently and selectively strips diverse sialoglycans from breast cancer cells. In syngeneic breast cancer models, desialylation enhanced immune cell infiltration and activation and prolonged the survival of mice, an effect that was dependent on expression of the Siglec-E checkpoint receptor found on tumor-infiltrating myeloid cells. Thus, antibody-sialidase conjugates represent a promising modality for glycoimmune checkpoint therapy.**

Immune checkpoint inhibitor (ICI) therapies have revolutionized treatment of certain cancers. For example, blocking antibodies against PD-1, PD-L1 and CTLA-4, have eradicated metastatic tumors in some patients, leading to long-term survival<sup>1,2</sup>. Although immune activation can be lifesaving, most patients do not respond or relapse after an initial response and the underlying mechanisms of primary and secondary resistance are not well understood<sup>3</sup>. Additional immune modulators might be at play, including alternative T cell checkpoints (for example, TIM-3, LAG-3 and A2AR), innate immune receptors and ligands (for example, CD47 and SIRP $\alpha$ ), and enzymes (for example, IDO and ADAR1). Several of these targets are under clinical evaluation, often in combination with a PD-1/PD-L1 blockade<sup>4</sup>.

While most ICIs target protein checkpoints<sup>4</sup>, cell-surface glycosylation has recently garnered interest as a mediator of immune inhibition<sup>5</sup>. This is supported by several decades of literature that have identified altered glycosylation as a hallmark of malignancy<sup>6,7</sup>. One example of a glycosylation pattern associated with cancer transformation is an increase in sialic acid-containing proteins and lipids (sialoglycans), a phenotype that intensifies with tumor progression and enhances tumor growth only in the context of an intact immune system in mice<sup>8–10</sup>. Subsequent work has demonstrated that sialoglycans suppress immune activation and act as glycoimmune checkpoints through multiple mechanisms: preventing complement-dependent cytotoxicity<sup>11</sup>, inhibiting immune-mediated apoptosis through the Fas death receptor<sup>12</sup>, masking immune-activating ligands of the natural killer (NK) cell receptor NKG2D<sup>8</sup>, preventing calreticulin binding and subsequent macrophage clearance<sup>13</sup> and directly binding sialic acid-binding immunoglobulin-like lectin (Siglec) receptors. In particular, the Siglec-sialoglycan axis of immune modulation is emerging as an important mediator of sialic acid-induced immune suppression in the context of cancer<sup>14</sup>.

The Siglec receptor family binds to a variety of sialoglycan structures and populates, often in combination, every immune cell class<sup>15,16</sup>. Eight family members (Siglecs-3, 5, 6, 7, 8, 9, 10 and 11) have intracellular domains that bear homology to that of PD-1 (ref. <sup>17</sup>), including an immunoreceptor tyrosine-based inhibition motif (ITIM) preceding a switch motif (ITSM) (Fig. 1a,b and Extended Data Fig. 1). These cytosolic ITIM/ITSM domains recruit protein tyrosine phosphatases, ultimately resulting in inhibitory signaling and immune cell suppression<sup>15,18</sup>. Thus, we and others speculated that Siglec engagement of cell-surface sialoglycans has inhibitory consequences similar to PD-1 engagement of PD-L1 (refs. <sup>19,20</sup>). In support of this hypothesis, Siglec-9 was recently shown to be upregulated on tumor-infiltrating T cells and correlated with reduced survival of patients with cancer<sup>10</sup>. Reciprocally, reduction of Siglec ligands through genetic knockout or inhibition of tumor sialic acid synthesis enhanced immune infiltration and reduced tumor growth<sup>10,21</sup>. The sialoglycan axis may therefore be a main contributor to tumor immune suppression and an attractive target for cancer immune therapy.

Sialoglycan ligands exhibit substantial chemical heterogeneity and are fused to a wide range of cell-surface protein and lipid scaffolds. Development of ligand-sequestering antibodies (analogous to PD-L1 blockade as illustrated in Fig. 1c) is therefore challenging. Thus, we previously conceived of a targeted degradation strategy wherein a sialic acid-cleaving enzyme (sialidase) was fused to a HER2-targeting antibody trastuzumab (Fig. 1d,e) to catalytically degrade sialoglycans in a tumor-specific manner<sup>22</sup>.

Here, we advance this strategy to full proof-of-concept by demonstrating that removal of sialoglycans from cancer cells using antibody-sialidase conjugates can improve the antitumor immune response in mice through a Siglec-E-dependent mechanism. These efforts necessitated rational design and screening for optimal sialidase activity to yield a trastuzumab-sialidase conjugate 2 (T-Sia 2)

<sup>1</sup>Department of Chemistry, Stanford University, Stanford, CA, USA. <sup>2</sup>Cancer Immunology Laboratory, Department of Biomedicine, University Hospital, Basel, Switzerland. <sup>3</sup>Division of Oncology, Department of Internal Medicine, University Hospital, Basel, Switzerland. <sup>4</sup>Department of Bioengineering, Stanford University, Stanford, CA, USA. <sup>5</sup>Howard Hughes Medical Institute, Stanford University, Stanford, CA, USA. ✉e-mail: [bertozzi@stanford.edu](mailto:bertozzi@stanford.edu)

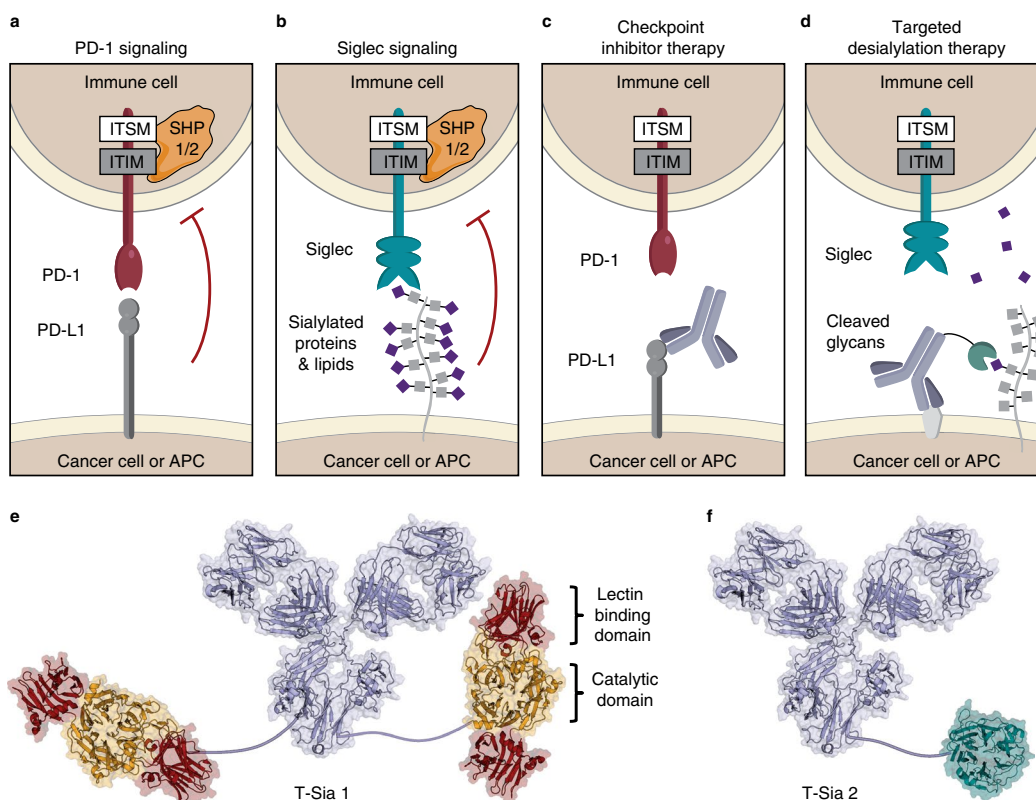


**Fig. 1 | Targeted desialylation of Siglec ligands with the antibody-enzyme conjugate T-Sia 2 as a modality for immune therapy.** **a, b**, PD-1 (**a**) and Siglecs (**b**) are receptors that typically suppress immune cell function on ligand binding. Engagement of PD-1 and Siglec receptors leads to recruitment of SHP phosphatases to the cytosolic ITIM/ITSM domains and inhibits immune cells. APC, antigen-presenting cell. **c**, PD-L1 checkpoint inhibitor therapy uses antibodies to bind PD-L1 and block extracellular interactions to PD-1, inhibiting SHP recruitment and enhancing the immune response to cancer. **d**, Targeted desialylation with an antibody-sialidase conjugate catalytically removes a chemically diverse group of Siglec ligands and prevents SHP recruitment to the Siglec ITIM/ITSM domains. **e**, Representation of previously reported T-Sia 1, in which trastuzumab was conjugated to two molecules of VC sialidase. **f**, Illustration of T-Sia 2, where trastuzumab is linked to an average of one ST sialidase. Trastuzumab is represented by mouse IgG1 PDB 1IGY; VC sialidase, 1WOP and ST sialidase, 3SIL.

(Fig. 1f), a sialoglycan degrader that exhibits a low off-target activity and high chemical stability needed for in vivo use. In a syngeneic orthotopic HER2<sup>+</sup> breast cancer model, targeting glycoimmune checkpoints with T-Sia 2 delayed tumor growth and enhanced immune infiltration, leading to prolonged survival of mice with trastuzumab-resistant breast cancer.

## Results

**Minimizing off-target sialidase activity.** We previously reported on an antibody-sialidase molecule, T-Sia 1 (Fig. 1e), constructed by conjugation of *Vibrio cholerae* (VC) sialidase to each trastuzumab heavy chain (chemical conjugation strategy described in Supplementary Fig. 1)<sup>22</sup>. Although T-Sia 1 efficiently cleaved sialoglycans from HER2<sup>+</sup> cells at low doses, the conjugate had considerable trastuzumab-independent activity as well<sup>22</sup>, which we ascribed to the low apparent  $K_M$  value of VC sialidase with polyvalent substrates (including cell surfaces)<sup>23</sup>. This attribute reflects the engagement of VC sialidase's two lectin domains (Fig. 1e), which enable cell-surface binding independent of antibody targeting<sup>23</sup>.

Accordingly, our first goal was to identify a more suitable sialidase from a repertoire that lacks such lectin domains. We expressed six recombinant bacterial and human sialidases in *Escherichia coli* (Extended Data Fig. 2a). The sialidases were screened for in vitro enzymatic activity and for their ability to enhance NK cell-mediated antibody-dependent cellular cytotoxicity (ADCC) against BT-20 breast cancer cells (Extended Data Fig. 2b,c). The *Salmonella typhimurium* (ST) sialidase NanH was selected for its relatively

high  $K_M$  value (mM range) against polyvalent targets<sup>23–25</sup>, enhancement of NK cell-mediated ADCC, and stability (Extended Data Fig. 2b–d). To ensure that ST sialidase would cleave Siglec-binding sialoglycans on breast cancer cells, we performed flow cytometry assays using Siglec-9-Fc and Siglec-7-Fc fusion proteins as probes. Treatment of nine different breast cancer cell lines with ST sialidase reduced Siglec-9-Fc and Siglec-7-Fc binding signal by >96% and >50%, respectively (Extended Data Fig. 2e–g). As postulated, ST sialidase on its own was less efficient than VC sialidase at removing sialoglycans from the cell surface (half-maximum effective concentration ( $EC_{50}$ ) > tenfold higher) (Fig. 2a and Supplementary Fig. 2).

To determine whether ST sialidase could be rendered selectively active by cell-surface targeting, we conjugated the enzyme to trastuzumab using a similar strategy as previously reported<sup>22</sup>, but in this case the ST sialidase was modified at a recombinantly inserted Cys residue (Supplementary Fig. 3a,b and 4a). The enzymatic activity of the sialidase, as measured with a fluorogenic substrate, was retained after conjugation to trastuzumab (Supplementary Fig. 4b). We next compared the activity and selectivity of the trastuzumab-ST sialidase conjugate to T-Sia 1 in a coculture assay comprising HER2<sup>+</sup> SK-BR-3 and HER2<sup>-</sup> MDA-MB-468 cells. Using the lectin *Sambucus nigra* agglutinin (SNA) as a probe for cell-surface sialoglycans, both conjugates desialylated HER2<sup>+</sup> target cells at concentrations near trastuzumab's reported  $K_D$  of 5 nM (Fig. 2b)<sup>26</sup> by flow cytometry. However, T-Sia 1 caused substantial off-target desialylation of MDA-MB-468 cells with an  $EC_{50}$  of 38 nM, whereas the trastuzumab-ST sialidase completely abrogated off-target reactivity

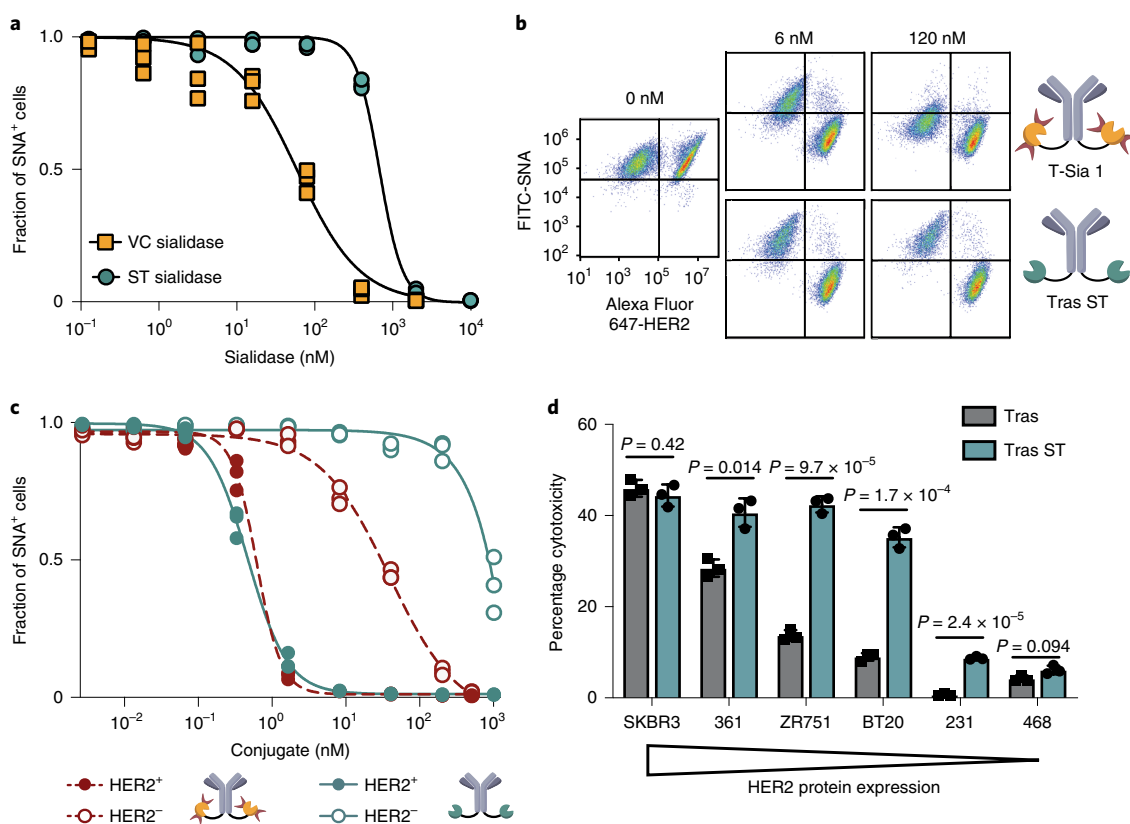


**Fig. 2 | ST sialidase cleaves sialic acid and enhances NK cell-mediated ADCC of HER2<sup>+</sup> cells with reduced off-target desialylation of HER2<sup>-</sup> cells.**

**a**, MDA-MB-468 cells were treated with sialidasases at various concentrations and stained with an SNA-fluorescein isothiocyanate (SNA-FITC) probe. Flow cytometry gating quantified the fraction of SNA<sup>+</sup> (sialylated) cells and the results were fit to a four-parameter variable slope. **b**, Representative flow cytometry dot plots from  $n = 3$  independent experiments of HER2<sup>+</sup> (SK-BR-3) and HER2<sup>-</sup> (MDA-MB-468) cells treated with T-Sia 1 or trastuzumab-ST sialidase conjugate (tras ST). **c**, Fraction of sialylated (SNA<sup>+</sup>) cells quantified by flow cytometry gating after treatment with various concentrations of antibody-sialidase conjugates and fit to a variable four-parameter slope. **d**, Breast cancer cell lines were treated with 10 nM trastuzumab-ST sialidase conjugate (tras ST) or trastuzumab (tras) and mixed with IL-2 activated human NK cells at E/T = 8 and NK cell-mediated ADCC was quantified by LDH assay after 4 h. Mean  $\pm$  s.d. is reported along with multiplicity-adjusted  $P$  values from two-tailed  $t$ -tests with the Holm-Sidak correction at  $\alpha = 0.05$ . All figures represent  $n = 3$  independent experimental replicates.

at that concentration ( $EC_{50}$  of  $\sim 1 \mu\text{M}$ ) (Fig. 2c and Supplementary Fig. 4c). Furthermore, the ST sialidase conjugate retained the ability to enhance NK cell-mediated ADCC of cells expressing medium and low levels of HER2 (Fig. 2d and Supplementary Fig. 5a,b). As expected, the highly trastuzumab-sensitive HER2-high SK-BR-3 cell line delivers a sufficiently strong activating signal to NK cells via Fc $\gamma$ RIII; therefore, removal of the inhibitory Siglec signal and enhancement of NKG2D binding provides no added benefit<sup>22</sup>. In summary, antibody conjugation to a sialidase with low intrinsic binding ability retains on-target sialidase activity while increasing the ‘therapeutic window’ of desialylation from 60-fold (T-Sia 1) to 2,000-fold.

**Optimizing the chemical stability of T-Sia 2.** Several advances to the construct design were required to enable in vivo examination of our conjugates. Specifically, the oxime bond used to conjugate trastuzumab to VC sialidase in T-Sia 1 is prone to hydrolysis in biological settings (Supplementary Fig. 1)<sup>27,28</sup>. We previously developed the Pictet–Spengler ligation, that forms a stable C–C adduct with SMARTag (aldehyde)-modified proteins<sup>27,29</sup>. More recently, a related process termed the hydrazino-*iso*-Pictet–Spengler (HIPS) reaction was developed<sup>30</sup>. An antibody–HIPS–maytansinoid conjugate demonstrated a long serum half-life and had the highest tolerated dose of any maytansinoid antibody–drug conjugate reported<sup>31</sup>, enabling advancement into human clinical studies. Based on these

precedents, we synthesized a HIPS–azide linker (1) (Supplementary Fig. 6) and conjugated this to SMARTag-labeled trastuzumab with full conversion detected by mass spectrometry (Fig. 3a and Supplementary Fig. 7a–c). We confirmed the enhanced stability of the HIPS–conjugated trastuzumab over the oxime linkage in human plasma and on live cells (Supplementary Fig. 8a–e).

To improve the uniformity of the trastuzumab–ST conjugate, we selectively and stably alkylated the engineered C-terminal Cys residue of ST sialidase with an  $\alpha$ -chloroacetamide–dibenzocyclooctyne (DBCO) linker (2) (Fig. 3a and Supplementary Fig. 9) under mild reducing conditions (Supplementary Fig. 10a). We confirmed that the engineered Cys residue was uniquely modified, with no off-target reactivity toward the four endogenous ST sialidase Cys residues (Supplementary Fig. 10b–d). Trastuzumab–azide and ST sialidase–DBCO were coupled by copper-free click chemistry<sup>32</sup> to produce T-Sia 2 (Fig. 3a).

Finally, we isolated T-Sia 2 fractions with enzyme/antibody ratios (EARs) of  $\sim 1$  and  $\sim 2$  by size exclusion chromatography (Supplementary Fig. 11a). In NK cell-mediated ADCC assays, T-Sia 2 with an EAR of  $\sim 1$  outperformed the EAR of  $\sim 2$  by a small but significant margin (1.13-fold increase,  $P = 0.035$ ) (Supplementary Fig. 11b, c). Accordingly, we optimized our conjugation procedure to increase the proportion of T-Sia 2 with an EAR of  $\sim 1$ . We characterized the conjugate by SDS–PAGE (Fig. 3b) and mass spectrometry (Supplementary Fig. 12a) and determined an EAR

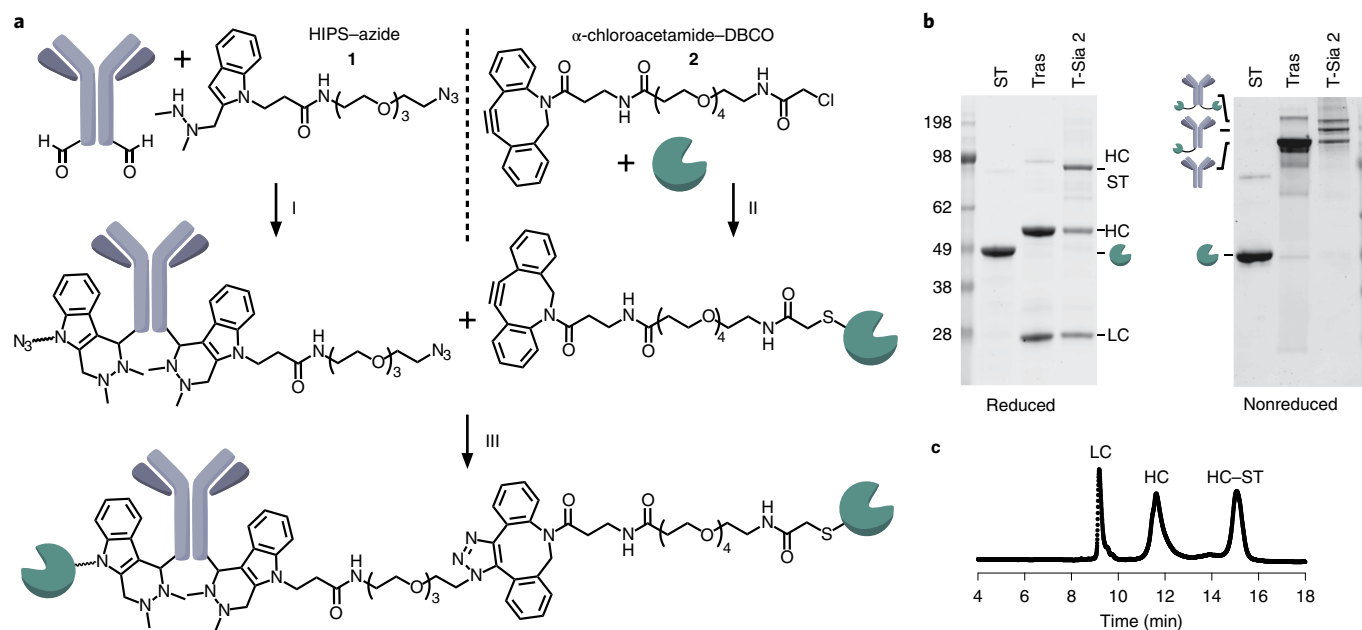


**Fig. 3 | Synthesis of T-Sia 2.** **a**, T-Sia 2 scheme: (i) Trastuzumab with heavy-chain formylglycine residues was reacted with 20 equiv. HIPS-azide **1** in citrate buffer pH 5.5. (ii) ST sialidase was site-selectively reacted with 20 equiv.  $\alpha$ -chloroacetamide-DBCO **2** under mildly reducing conditions. (iii) Sialidase-DBCO and trastuzumab-azide were coupled via copper-free click chemistry to form T-Sia 2. **b**, SDS-PAGE gel with nonreducing buffer (left) and reducing buffer (right) of sialidase-DBCO, trastuzumab-HIPS-azide and T-Sia 2; data is representative of  $n=3$  independently run gels. **c**, Representative HPLC trace from  $n=3$  independent experimental replicates of T-Sia 2, absorbance detected at 280 nm. LC, antibody light chain; HC, antibody heavy chain; HC-ST, antibody heavy chain conjugated to ST sialidase.

of 0.9 by high-performance liquid chromatography (HPLC) analysis (Fig. 3c). We confirmed that T-Sia 2 binds its antigen HER2 and mouse Fc receptors similarly to trastuzumab (Supplementary Fig. 12b,c), and still enhances NK cell- and  $\gamma\delta$  T cell-mediated ADCC (Extended Data Fig. 3a–i).

**T-Sia 2 delays HER2<sup>+</sup> tumor growth in mice.** For in vivo testing of T-Sia 2, we selected the syngeneic orthotopic mouse EMT6 mammary carcinoma model<sup>33</sup>, in which the EMT6 cell line was engineered to express HER2 yet remained resistant to trastuzumab monotherapy in mice<sup>34</sup>. In vitro, ST sialidase cleaved sialoglycans from HER2<sup>+</sup> EMT6 cells, causing a decrease in binding to both human and mouse Siglec-Fc fusion probes (Supplementary Fig. 13) and T-Sia 2 enhanced human NK cell-mediated ADCC (Fig. 4a).

Next we performed in vivo experiments as depicted in Fig. 4b. HER2<sup>+</sup> EMT6 cells were injected into the mammary fat pads of mice followed by intraperitoneal (i.p.) treatment with phosphate-buffered saline (PBS), trastuzumab or T-Sia 2. After 28 d, all mice in the PBS and trastuzumab-treated groups had reached a tumor burden requiring euthanasia (Fig. 4c,d). In contrast, T-Sia 2 at both doses extended mouse survival to 40 d and demonstrated substantial tumor growth delay compared to trastuzumab or PBS alone (Fig. 4c,d and Extended Data Fig. 4a). No difference in tumor growth was observed between the two doses of T-Sia 2 (Fig. 3c), and although the 10 mg kg<sup>-1</sup> dose of T-Sia 2 was well tolerated in terms of weight loss, the 15 mg kg<sup>-1</sup> dose resulted in a minimal (<10%) weight loss compared to PBS-treated mice at day 24 (Extended Data Fig. 4b). Lectin staining of tumor suspensions with peanut agglutinin (PNA), which binds to galactose residues exposed on sialidase treatment, showed increased labeling in the T-Sia 2-treated tumors compared to the PBS- or trastuzumab-treated mice detectable 13–23 d after the final conjugate injections (Extended Data Fig. 4c). These data indicate that T-Sia 2 desialylated the tumor microenvironment (TME) and slowed the progression of EMT6 tumor growth in mice.

**T-Sia 2 depletes HER2<sup>+</sup> tumor sialoglycans in vivo.** To determine whether T-Sia 2 preferentially accumulates in and destroys sialoglycans from the HER2<sup>+</sup> tumors in mice, we first modified the conjugate with IRDye 800CW (IR800) NHS ester and imaged mice bearing subcutaneous (s.c.) EMT6 tumors treated with a single injection of 500 (~5 mg kg<sup>-1</sup>), 100 or 20 pmol of the IR800-labeled T-Sia 2 or PBS control (Fig. 4e). After 48 h, tumors on the left flank of the anesthetized mice were fluorescent at the highest dose (Extended Data Fig. 5a). After 4 d, mice were killed to further analyze T-Sia 2 localization and activity in individual organs. Both the 500- and 100-pmol doses of IR800-labeled T-Sia 2 accumulated in tumors; however, the higher dose also showed fluorescence accumulation in the liver and kidneys, likely involved in antibody and fluorophore clearance (Extended Data Fig. 5b–d). All T-Sia 2 doses appeared to degrade tumor sialoglycans; flow cytometry of resuspended tumors demonstrated no notable change by SNA, but decreased Maackia Amurensis Lectin II (MALII) binding, which preferentially binds sialic acid in an ( $\alpha$ -2,3) linkage, as well as increased unmasked galactose detected with PNA (Extended Data Fig. 5e). Lectin histology and imaging was also performed at the 500-pmol dose to visualize desialylation of the mouse tissues. Although tumors showed the most striking desialylation, all of the tissues analyzed showed evidence of sialoglycan degradation by MALII and PNA (Extended Data Fig. 6), indicating that the higher doses of antibody-sialidase conjugates in the tumor growth studies were desialylating tissues throughout the mice.

**Isotype-Sia, FcX-Sia and T-Sia-LOF control molecules.** To better understand the mechanisms underlying T-Sia 2's antitumor activity, we synthesized three control molecules using the same conjugation strategy as with T-Sia 2 (Fig. 5a). The first was T-Sia 2 in which the sialidase's catalytic nucleophile was mutated (Y→A), causing loss of function (T-Sia-LOF) (Supplementary Fig. 14). The second was an isotype control human IgG1-sialidase conjugate with the antibody

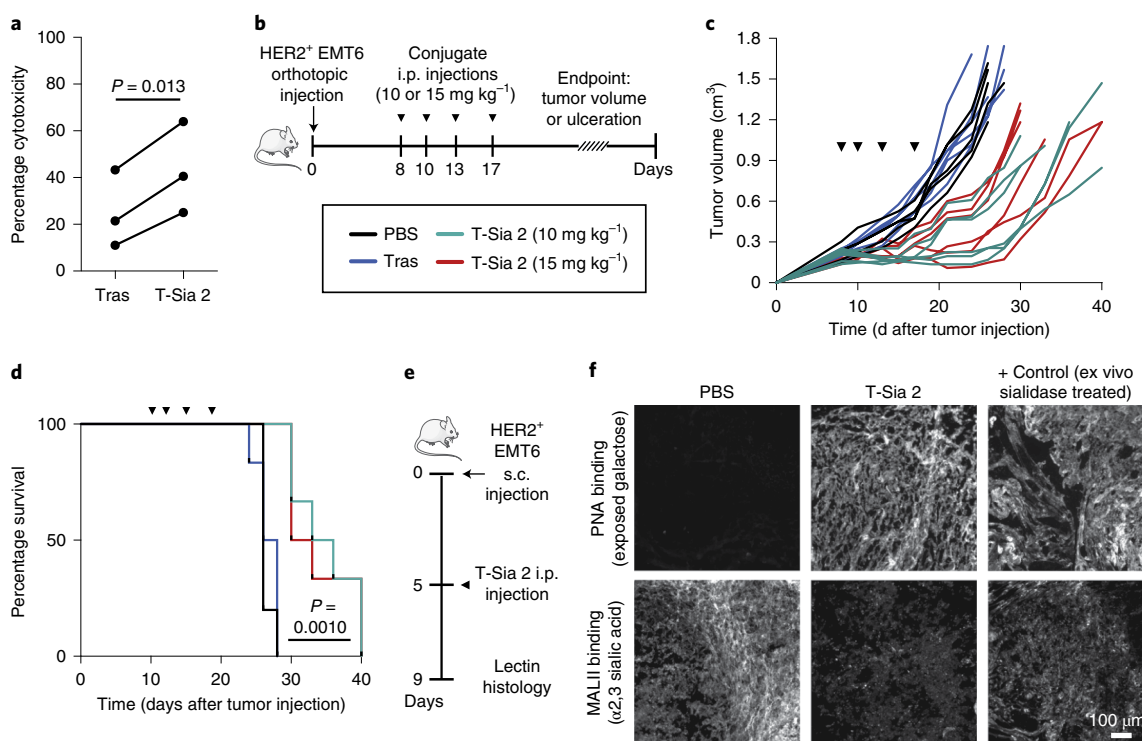


**Fig. 4 | T-Sia 2 degrades sialoglycans and slows tumor growth in a HER2<sup>+</sup> EMT6 syngeneic mouse breast cancer model that is resistant to trastuzumab alone.** **a**, HER2<sup>+</sup> EMT6 cells were treated with PBS, 10 nM trastuzumab (Tras) or 10 nM of T-Sia 2. Human NK cells were added at a ratio of 3:1 and ADCC was quantified by flow cytometry after 4 h and subtracting PBS controls. A paired two-tailed *t*-test is shown for  $n = 3$  independent biological replicates of different NK cell donors. **b**, HER2<sup>+</sup> EMT6 cells were injected into the mammary fat pad of Balb/c mice. Starting on day 8, mice were injected i.p. every 2–4 d with PBS ( $n = 5$ ), trastuzumab (Tras, 15 mg kg<sup>-1</sup>,  $n = 6$ ) or T-Sia 2 (10 or 15 mg kg<sup>-1</sup>,  $n = 6$ ). **c**, Individual growth curves of the HER2<sup>+</sup> EMT6 tumors in mice. **d**, Survival curve for animals described in **b**; statistics were a log-rank (Mantel-Cox) test comparing T-Sia 2 (10 mg kg<sup>-1</sup>) with trastuzumab. **e**, For T-Sia 2 histology, s.c. HER2<sup>+</sup> EMT6 were injected, followed by i.p. injection of T-Sia 2 or PBS at day 5 and killed on day 9. **f**, Fluorescent images of tumor slices of the mice treated in **e**, with PBS, 500 pmol (~5 mg kg<sup>-1</sup>) T-Sia 2, or a positive control of tumor slices treated ex vivo with a sialidase cocktail. Slides were stained with biotinylated PNA or MALII lectin followed by streptavidin-647. Images are representative of an experiment with  $n = 3$  mice per group; scale bar, 100 μm, lower-right image, more images from this experiment are in Extended Data Fig. 6.

motavizumab that targets an antigen not present in laboratory mice (respiratory syncytial virus) and has 87% identity to trastuzumab (Isotype-Sia) (Supplementary Fig. 15)<sup>35,36</sup>. The third was a variant possessing several point mutations (ELLG→PVA-) in the Fcγ receptor (FcγR) binding domain of trastuzumab, which abolishes most effector FcγR interactions on immune cells while maintaining most of the neonatal Fc receptor (FcRn) binding and therefore native antibody recycling (T-FcX-Sia) (Supplementary Fig. 16)<sup>37,38</sup>. In vitro NK cell-mediated ADCC assays with several HER2<sup>+</sup> cell lines demonstrated that T-Sia 2 was superior in eliciting cell death whereas T-Sia-LOF had comparable activity to trastuzumab alone (Fig. 5b and Supplementary Fig. 17). As expected, Isotype-Sia was ineffective in stimulating ADCC against HER2<sup>+</sup> cells and T-FcX-Sia had greatly diminished ADCC activity compared to T-Sia 2 in vitro.

**HER2 targeting improves tumor desialylation in vivo.** Since Isotype-Sia is expected to circulate throughout the mice, and since T-Sia 2 degrades sialoglycans in off-target mouse organs at a 500-pmol dose (Extended Data Fig. 6), we anticipated that the untargeted Isotype-Sia may also desialylate the TME. We were interested to test whether HER2<sup>+</sup> targeting by T-Sia 2 could improve tumor degradation of sialic acids over untargeted Isotype-Sia in vivo. If so, we hypothesized that this effect would be most discernable at a low dose; therefore, we injected a 20-pmol dose of T-Sia 2, Isotype-Sia or PBS as depicted in Fig. 5c. After 4 d, tumors were harvested and analyzed for lectin binding by flow cytometry. Consistent with the previous results, T-Sia 2-treated

mice had desialylated tumors measurable by flow cytometry with PNA and MALII staining (Fig. 5c), but not by SNA staining in vivo (Extended Data Fig. 7a). Isotype-Sia-treated tumors had substantially more tumor sialoglycans than T-Sia 2 (Fig. 5c), indicating that targeting with trastuzumab can improve sialoglycan degradation in the TME.

**T-Sia 2 therapy requires active ST Sia but not FcγR.** The antibody-sialidase conjugates were then injected i.p. into Balb/c mice bearing established HER2<sup>+</sup> EMT6 tumor cells in their mammary fat pads (Fig. 5d). Consistent with the previous mouse experiment, T-Sia 2-treated mice had prolonged survival and slow tumor growth compared to PBS- and trastuzumab-treated mice (Fig. 5d,e and Extended Data Fig. 7b,c). Survival and tumor growth of T-Sia-LOF-treated mice was not notably different from trastuzumab- or PBS-treated mice, indicating that sialidase activity mediates the therapeutic effect (Fig. 5d,e and Extended Data Fig. 7c). T-Sia 2-treated mice showed a slight early delay in tumor growth that was not evident in T-FcX-Sia-treated mice (Extended Data Fig. 7c); however, there was no significant difference in survival between the two treatment groups (Fig. 5e,  $P = 0.89$ ). The early tumor growth differences suggest that T-Sia 2 may be potentiating both FcγR-dependent and -independent immune responses in mice; however, the strong survival benefit of T-FcX-Sia indicates that T-Sia 2's principle mechanism of action in vivo is not dependent on enhancing ADCC or antibody-dependent cellular phagocytosis (ADCP) through antibody-Fcγ receptor binding.

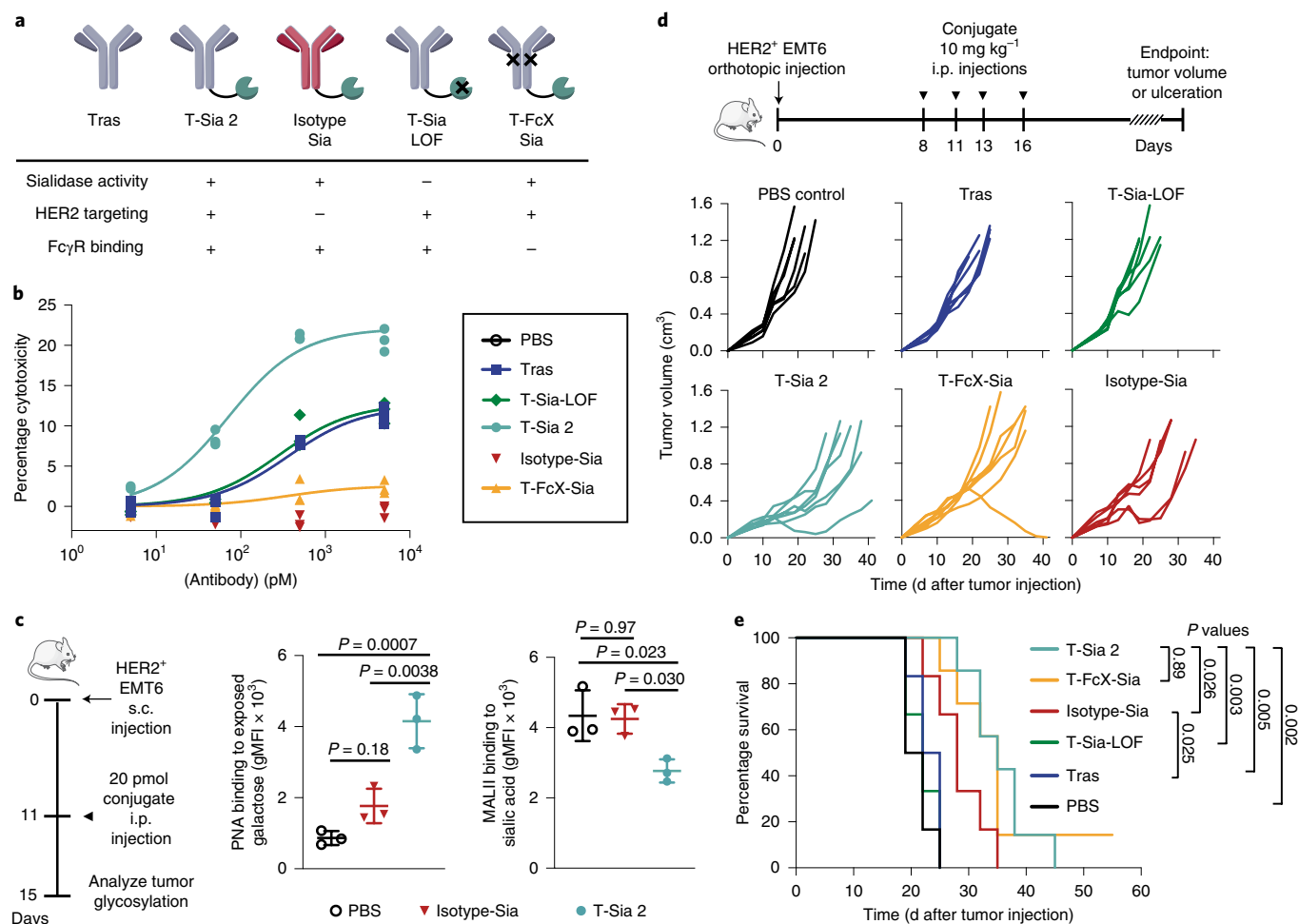


**Fig. 5 | Active sialidase is essential for T-Sia 2 efficacy in mice and HER2 targeting is advantageous, but antibody-Fc $\gamma$ R recruitment and ADCC are negligible contributors to an anticancer immune response with sialoglycan degraders in vivo.** **a**, Schematic of the antibody-sialidase conjugate controls. **b**, NK cell-mediated ADCC of ZR-75-1 cancer cells treated with antibody conjugates, E/T=3, detecting percentage cytotoxicity by LDH release after 8 h of  $n=3$  experimental replicates, a one-site-specific binding least-squares fit was modeled onto the data with GraphPad Prism. **c**, For flow cytometry analysis, a single 20-pmol injection of T-Sia 2, Isotype-Sia or PBS control was injected i.p. into mice with s.c. HER2<sup>+</sup> EMT6 cells. Tumors were harvested 4-d postinjection. Flow cytometry with PNA, which binds to galactose residues exposed on sialidase treatment is shown on the left and MALII binding of  $\alpha$ -2,3-linked sialic acid is shown on the right for  $n=3$  mice per group, geometric mean  $\pm$  s.d., analyzed by ordinary one-way ANOVA with multiplicity-adjusted  $P$  values from Tukey's multiple comparisons test. **d**, HER2<sup>+</sup> EMT6 cells were injected into the mammary fat pad of Balb/c mice. Mice were injected i.p. with PBS ( $n=6$ ), 10 mg kg<sup>-1</sup> of trastuzumab (tras) ( $n=6$ ), T-Sia-LOF ( $n=6$ ), Isotype-Sia ( $n=6$ ), T-FcX-Sia ( $n=7$ ) or T-Sia 2 ( $n=7$ ), every 2-4 d for four total injections. Individual tumor growth curves for these mice are shown until day 41. **e**, Kaplan-Meier plot of the survival based on euthanasia criteria of mice in **d** with  $P$  values from log-rank (Mantel-Cox) tests shown.

Tumor growth in mice treated with the Isotype-Sia was heterogeneous (Fig. 5d), as was tumor PNA lectin staining at time of death (Extended Data Fig. 7d), indicating that mice treated with Isotype-Sia at high 10 mg kg<sup>-1</sup> concentrations also had sialoglycan degradation in the tumors. Perhaps because of this, the Isotype-Sia molecule was moderately effective and prolonged survival compared to trastuzumab-treated mice ( $P=0.025$ , Fig. 5e). The efficacy of this molecule in mice corroborates the T-FcX-Sia findings that the primary mechanism of action of T-Sia 2 is not mediated by ADCC/ADCP in vivo, as Isotype-Sia did not mediate in vitro NK cell-mediated ADCC. Nevertheless, targeted accumulation of the sialidase activity to the tumors with T-Sia 2 prolonged survival compared to Isotype-Sia ( $P=0.026$ , Fig. 5e).

**TME and blood cell changes in T-Sia 2-treated mice.** To further investigate effects of sialidase exposure, we analyzed blood cell counts pursuant to administration of the previously mentioned antibody-sialidase conjugates. Forty-eight hours after the

first injection of conjugates, red and white blood cell counts were comparable to PBS-treated controls (Supplementary Fig. 18a,b), whereas the platelet count decreased to an average of 157 platelets per nl of blood in mice treated with any construct containing active sialidase (Supplementary Fig. 18c), likely mediated by the asialoglycoprotein receptor in the liver that binds to exposed galactose on platelet desialylation<sup>39,40</sup>. Thrombocytopenia is a common symptom of cancer treatment and some platelet loss may be a favorable prognostic biomarker of ICI therapy<sup>41</sup>. Encouragingly, none of the sialidase conjugates instigated weight loss or signs of ill health in treated mice (Supplementary Fig. 18d).

Tumors of PBS, trastuzumab and T-Sia 2-treated mice were collected at survival endpoints and the infiltrating immune cells were extracted and analyzed by flow cytometry. The results from the combined mouse experiments showed an increase in total tumor leukocytes in the T-Sia 2-treated mice compared to PBS- and trastuzumab-treated mice (Supplementary Fig. 19a). Additionally, T-Sia 2 treatment augmented the ratio of CD8<sup>+</sup> T cells to T<sub>reg</sub> cells

(Supplementary Fig. 19b), an indicator of improved patient prognosis in breast cancer<sup>42</sup>. Other immune marker changes in the T-Sia 2-treated tumors included an increase in MHCII<sup>+</sup> tumor associated macrophages and a decrease in CD206<sup>+</sup> tumor associated macrophages (Supplementary Fig. 19c,d) compared to PBS-treated mice, indicating a potential switch to a more inflammatory macrophage polarization<sup>43</sup>. Additionally, T-Sia 2-treated tumors had increased activated (CD69<sup>+</sup>, Supplementary Fig. 19e,f) and cytotoxic (granzyme b<sup>+</sup>, Supplementary Fig. 19g,h) CD8<sup>+</sup> T and NK cells. Further tumor infiltrating leukocyte (TIL) analyses and flow cytometry gating are shown in Supplementary Figs. 20 and 21.

**T-Sia 2 inhibits the glycoimmune checkpoint Siglec-E.** Recent evidence suggests that Siglec-E (a mouse homolog of human Siglec-7/-9) is the main Siglec present on the tumor-infiltrating CD8<sup>+</sup> T cells of several murine cancer models including the EMT6 tumor model in mice<sup>10</sup>. We therefore hypothesized that Siglec-E might be a contributor to the immunosuppressive phenotype and that destroying Siglec-E ligands is an important mechanism of action of T-Sia 2 in mice. As there are no currently available fully antagonistic blocking antibodies for Siglec-E, we tested T-Sia 2 in C57BL/6 mice lacking inhibitory Siglec-E (Sig-E<sup>-/-</sup>)<sup>44</sup>.

The HER2<sup>+</sup> B16D5 melanoma tumor model is syngeneic in C57BL/6 mice, and expresses Siglec-E ligands that are cleavable by ST sialidase (Extended Data Fig. 8). Therefore, HER2<sup>+</sup> B16D5 cells were injected s.c. into the flanks of either wildtype (WT) or Sig-E<sup>-/-</sup> C57BL/6 mice. After 7 d, mice were treated with T-Sia 2 or the T-Sia-LOF control, and tumor growth was assessed (Fig. 6a). As expected, the sialoglycan degrader T-Sia 2 increased mouse survival and delayed tumor growth in WT mice (Fig. 6b and Extended Data Fig. 9a,b). In Sig-E<sup>-/-</sup> mice, there was no clear benefit of T-Sia 2 treatment over T-Sia-LOF (Fig. 6c and Extended Data Fig. 9b,c), indicating that the therapeutic effects of sialoglycan degradation *in vivo* are largely dependent on functional Siglec-E expression. Correspondingly, Sig-E<sup>-/-</sup> had slower HER2<sup>+</sup> B16D5 tumor growth and prolonged survival compared to WT mice treated with T-Sia-LOF, and there was no apparent survival benefit of Siglec-E knockout when mice were treated with T-Sia 2 (Extended Data Fig. 9b,d).

Finally, flow cytometry analysis of tumor-infiltrating leukocytes was performed on  $n=10$  HER2<sup>+</sup> B16D5 tumors grown in WT mice to identify the Siglec-E-expressing immune cells in the TME that might be contributing to the immunosuppressive phenotype. Tumors grown in Sig-E<sup>-/-</sup> mice ( $n=12$ ) were analyzed as a negative control (gating in Supplementary Fig. 22). An average of 17% of total leukocytes (CD45<sup>+</sup> cells) were positive for Siglec-E (Fig. 6d and Extended Data Fig. 10). While Siglec-E expression was not detected on CD45<sup>+</sup> subsets expressing CD19<sup>+</sup>, CD3<sup>+</sup> or NK1.1<sup>+</sup> cells (B cells, T cells and NK cells, respectively), most myeloid cells (CD11b<sup>+</sup> cells) a population including macrophages, myeloid dendritic cells, granulocytes and monocytes, stained positive for Siglec-E (Fig. 6d and Extended Data Fig. 10).

## Discussion

The correlation of hypersialylation with cancer progression was first reported in the 1960s (ref. 45). In the 1970s, researchers explored the effects of sialidase treatment for cancer therapy, but without the framework for a cogent mechanistic hypothesis and with mixed results likely due to questionable enzyme quality and rapid recovery of cell-surface sialic acid<sup>45</sup>. The development of modern techniques for bioconjugation, as well as recent breakthroughs in our understanding of the role of sialoglycans in immune modulation prompted us to explore whether tumor-targeted sialidase enzymes could now be effectively harnessed for cancer therapy. These efforts yielded T-Sia 2, a trastuzumab-ST sialidase conjugate that prolonged survival in a trastuzumab-resistant cancer model.

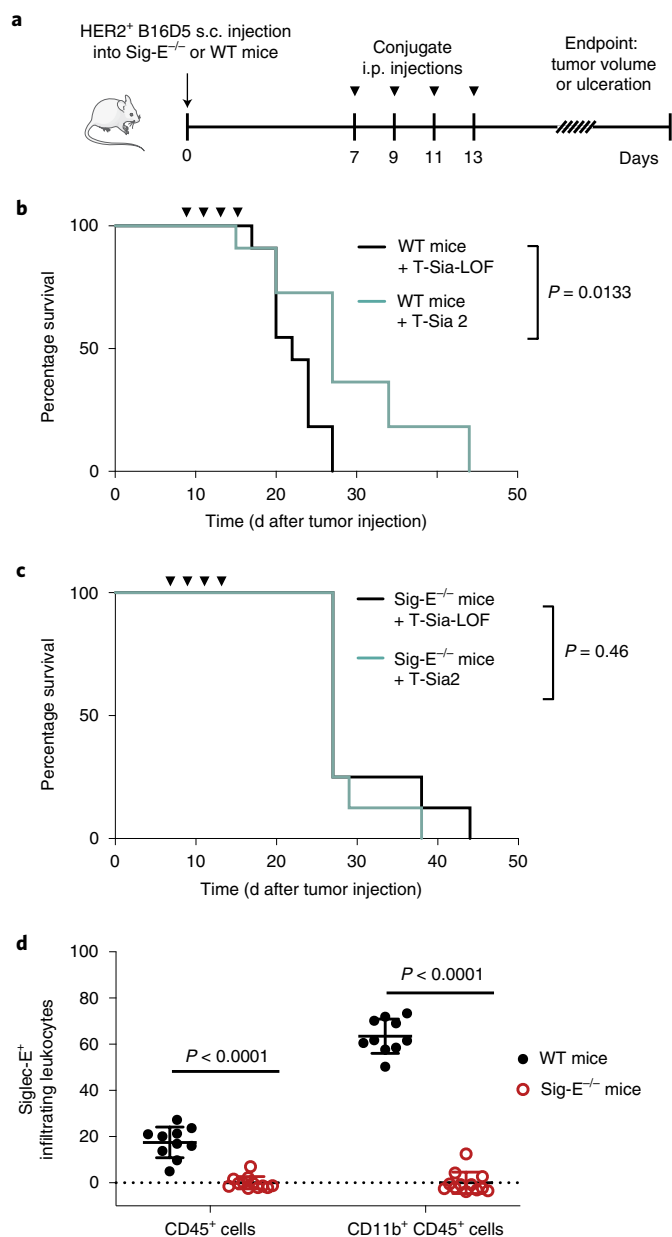


**Fig. 6 | T-Sia 2 therapy is dependent on functional Siglec-E, a receptor highly expressed on tumor-infiltrating myeloid cells.** **a–c**, HER2<sup>+</sup> B16D5 cells were injected s.c. **(a)** into either WT C57BL/6 mice **(b)** or Sig-E<sup>-/-</sup> C57BL/6 mice **(c)**. Mice were injected four times i.p. with 10 mg kg<sup>-1</sup> T-Sia 2 ( $n=11$  WT,  $n=8$  Sig-E<sup>-/-</sup>) or the inactive T-Sia-LOF ( $n=11$  WT,  $n=8$  Sig-E<sup>-/-</sup>). Survival curves are displayed indicating when euthanasia criteria were reached,  $P$  values are shown from a log-rank (Mantel-Cox) test. Data are from  $n=2$  independent mouse experiments and individual growth curves are reported in Extended Data Fig. 9. **d**, Percentage of tumor-infiltrating leukocytes (CD45<sup>+</sup>) and myeloid cells (CD11b<sup>+</sup> of CD45<sup>+</sup>) that are Siglec-E<sup>+</sup> by flow cytometry with background staining subtracted. Mean values  $\pm$  s.d. are reported along with multiplicity-adjusted  $P$  values from two-tailed  $t$ -tests with the Holm-Sidak correction at  $\alpha=0.05$  from  $n=10$  WT mice and  $n=12$  Sig-E<sup>-/-</sup> mice. Myeloid cells (CD11b<sup>+</sup>) can include macrophages, dendritic cells, monocytes and granulocytes.

The use of two bioorthogonal chemistry tools—a HIPS reaction with aldehyde-tagged antibodies and copper-free click chemistry—enabled modular assembly of conjugates using common functionalized antibody and enzyme moieties. Key factors in the performance

of T-Sia 2 were its target specificity and plasma stability imparted by antibody conjugation, which facilitated degradation of sialoglycans in the TME that was measurable weeks after conjugate injection.

T-Sia 2 was designed to desialylate the TME, remove Siglec ligands and thereby potentiate ADCC. However, we observed that T-Sia 2 was only effective in mice expressing the Siglec-E receptor, which was located on myeloid cells in the TME, and also that T-Sia 2 performs about equally to its ADCC/ADCP-impaired control molecule T-FcX-Sia. These data indicate that antibody effector functions are not critical for therapeutic effect in these mouse models. Many other immune mechanisms are suppressed by inhibitory Siglec signaling that could be at play, including direct macrophage phagocytosis<sup>46</sup>, cytokine production<sup>15</sup> and T cell receptor signaling and effector function<sup>47</sup>. Administration of T-Sia 2 enhanced the CD8<sup>+</sup> T cell/ T<sub>reg</sub> ratio and promoted an increase in activated NK cells and CD8<sup>+</sup> T cells. These results are consistent with reports that implicate NK cells<sup>8,9</sup> and CD8<sup>+</sup> T cells<sup>9,21</sup> as key mediators of the immune response against hyposialylated cancers. However, the B16D5 tumor-infiltrating NK and T cells did not express significant Siglec-E checkpoint receptor; consequently, this work also points to a critical role for mouse Siglec-E<sup>+</sup> CD11b<sup>+</sup> tumor-infiltrating myeloid cells in stimulating an immune response against desialylated tumors. Although Siglec-E binding is the primary glycoimmune checkpoint inhibited by T-Sia 2 in the B16D5 tumor model, tumor desialylation can improve immune response to cancer through many other mechanisms, including increasing complement-dependent cytotoxicity, promoting Fas receptor signaling, enhancing calreticulin binding and macrophage clearance, exposing NKG2D ligands and destroying the ligands of other Siglecs<sup>8,11–13</sup>.

Several human Siglecs have now been implicated as immune suppressors in the TME, including Siglecs 7, 9, 10 and 15 (refs. <sup>10,19,46,48,49</sup>) but the importance of their relative contributions may vary from tumor to tumor. Although the molecular details of their biological ligands remain an active area of research, these Siglec family members all recognize terminal sialoglycans and the chemical diversity and complexity of these ligands has made it challenging to generate targeted therapeutics with broadly neutralizing activity. The targeted degradation strategy exemplified herein offers a new modality to destroy such sialoglycans in a Siglec-agnostic manner. As well, we see targeted glycan degradation as a promising strategy for other diseases settings marked by pathologic glycosylation. Further study of Siglec-sialoglycan biology in a range of different cancer subtypes will be essential to elucidate the precise indications where sialidase conjugates such as T-Sia 2 may be most effective. Significantly, the modular chemical synthesis of T-Sia 2 can be readily adapted to other FDA-approved therapeutic monoclonal antibodies, allowing for simple and rapid targeting of sialidase enzymes to a wide range of tumor types.

While this study demonstrates some efficacy of T-Sia 2 as a monotherapy, there is significant future scope for combining antibody-sialidase molecules that target glycoimmune checkpoints with more traditional ICI therapies or antibody-drug conjugates (ADCs). Siglec receptors are expressed across a broad range of innate and adaptive immune cells and Siglec-9<sup>+</sup> CD8<sup>+</sup> TILs coexpress ICIs<sup>10,47</sup>, indicating that T-Sia 2 may have pan-immune synergy with other with immune checkpoint agents. Recent evidence also suggests that removal of surface sialic acid increases the internalization rate of ADCs, and targeted desialylation could enhance their cytotoxic effects<sup>30</sup>. We anticipate that glycan-editing antibody therapies will prove a potent tool among the wider arsenal of new anticancer therapies moving toward clinical translation.

### Online content

Any Nature Research reporting summaries, source data, extended data, supplementary information, acknowledgements, peer review information; details of author contributions and competing interests;

and statements of data and code availability are available at <https://doi.org/10.1038/s41589-020-0622-x>.

Received: 23 May 2019; Accepted: 8 July 2020;

Published online: 17 August 2020

### References

- Schadendorf, D. et al. Pooled analysis of long-term survival data from phase II and phase III trials of ipilimumab in unresectable or metastatic melanoma. *J. Clin. Oncol.* **33**, 1889–1894 (2015).
- Ribas, A. et al. Association of pembrolizumab with tumor response and survival among patients with advanced melanoma. *J. Am. Med. Assoc.* **315**, 1600–1609 (2016).
- Sharma, P., Hu-Lieskovan, S., Wargo, J. A. & Ribas, A. Primary, adaptive, and acquired resistance to cancer immunotherapy. *Cell* **168**, 707–723 (2017).
- Marin-Acevedo, J. A. et al. Next generation of immune checkpoint therapy in cancer: new developments and challenges. *J. Hematol. Oncol.* **11**, 39 (2018).
- Li, C.-W. et al. Eradication of triple-negative breast cancer cells by targeting glycosylated PD-L1. *Cancer Cell* **33**, 187–201 (2018).
- Boligan, K. F., Mesa, C., Fernandez, L. E. & von Gunten, S. Cancer intelligence acquired (CIA): tumor glycosylation and sialylation codes dismantling antitumor defense. *Cell. Mol. Life Sci.* **72**, 1231–1248 (2015).
- Varki, A., Kannagi, R., Toole, B. & Stanley, P. in *Essentials of Glycobiology* (Cold Spring Harbor Laboratory Press, 2017).
- Cohen, M. et al. Sialylation of 3-methylcholanthrene-induced fibrosarcoma determines antitumor immune responses during immunoeediting. *J. Immunol.* **185**, 5869–5878 (2010).
- Perdicchio, M. et al. Tumor sialylation impedes T cell mediated anti-tumor responses while promoting tumor associated-regulatory T cells. *Oncotarget* **7**, 8771–8782 (2016).
- Stanczak, M. A. et al. Self-associated molecular patterns mediate cancer immune evasion by engaging Siglecs on T cells. *J. Clin. Invest.* **128**, 4912–4923 (2018).
- Varki, A. & Gagneux, P. Multifarious roles of sialic acids in immunity. *Ann. NY Acad. Sci.* **1253**, 16–36 (2012).
- Swindall, A. F. & Bellis, S. L. Sialylation of the Fas death receptor by ST6Gal-I provides protection against Fas-mediated apoptosis in colon carcinoma cells. *J. Biol. Chem.* **286**, 22982–22990 (2011).
- Feng, M. et al. Programmed cell removal by calreticulin in tissue homeostasis and cancer. *Nat. Commun.* **9**, 3194 (2018).
- Lübbbers, J., Rodríguez, E. & van Kooyk, Y. Modulation of immune tolerance via Siglec-Sialic acid interactions. *Front. Immunol.* **9**, 2807 (2018).
- Macauley, M. S., Crocker, P. R. & Paulson, J. C. Siglec-mediated regulation of immune cell function in disease. *Nat. Rev. Immunol.* **14**, 653–666 (2014).
- Paulson, J. C., Macauley, M. S. & Kawasaki, N. Siglecs as sensors of self in innate and adaptive immune responses. *Ann. NY Acad. Sci.* **1253**, 37–48 (2012).
- Riley, J. L. PD-1 signaling in primary T cells. *Immunol. Rev.* **229**, 114–125 (2009).
- Chemnitz, J. M., Parry, R. V., Nichols, K. E., June, C. H. & Riley, J. L. SHP-1 and SHP-2 associate with immunoreceptor tyrosine-based switch motif of programmed death 1 upon primary human T cell stimulation, but only receptor ligation prevents T cell activation. *J. Immunol.* **173**, 945–954 (2004).
- Läubli, H. et al. Engagement of myelomonocytic Siglecs by tumor-associated ligands modulates the innate immune response to cancer. *Proc. Natl Acad. Sci. USA* **111**, 14211–14216 (2014).
- Hudak, J. E., Canham, S. M. & Bertozzi, C. R. Glycocalyx engineering reveals a Siglec-based mechanism for NK cell immunoevasion. *Nat. Chem. Biol.* **10**, 69–75 (2014).
- Büll, C. et al. Sialic acid blockade suppresses tumor growth by enhancing T-cell-mediated tumor immunity. *Cancer Res.* **78**, 3574–3588 (2018).
- Xiao, H., Woods, E. C., Vukojicic, P. & Bertozzi, C. R. Precision glycocalyx editing as a strategy for cancer immunotherapy. *Proc. Natl Acad. Sci. USA* **113**, 10304–10309 (2016).
- Thobhani, S., Ember, B., Siriwardena, A. & Boons, G.-J. Multivalency and the mode of action of bacterial sialidases. *J. Am. Chem. Soc.* **125**, 7154–7155 (2003).
- Watson, J. N. et al. Use of conformationally restricted pyridinium-D-N-acetylneuraminides to probe specificity in bacterial and viral sialidases. *Biochem. Cell Biol.* **83**, 115–122 (2005).
- Minami, A. et al. Catalytic preference of *Salmonella typhimurium* LT2 sialidase for N-acetylneuraminic acid residues over N-glycolylneuraminic acid residues. *FEBS Open Bio.* **3**, 231–236 (2013).
- Shepard, H. M., Jin, P., Slamon, D. J., Pirot, Z. & Maneval, D. C. in *Therapeutic Antibodies* (eds. Chernajovsky, Y. & Nissim, A.) 183–219 (Springer, 2008).

27. Agarwal, P., van der Weijden, J., Sletten, E. M., Rabuka, D. & Bertozzi, C. R. A Pictet–Spengler ligation for protein chemical modification. *Proc. Natl Acad. Sci. USA* **110**, 46–51 (2013).
28. Agarwal, P. et al. Hydrazino-Pictet–Spengler ligation as a biocompatible method for the generation of stable protein conjugates. *Bioconjug. Chem.* **24**, 846–851 (2013).
29. Barfield, R. M. & Rabuka, D. *Noncanonical Amino Acids*. (ed. Lemke, E. A.) 3–16 (Humana Press, 2018).
30. Drake, P. M. et al. Aldehyde tag coupled with HIPS chemistry enables the production of ADCs conjugated site-specifically to different antibody regions with distinct in vivo efficacy and PK outcomes. *Bioconjug. Chem.* **25**, 1331–1341 (2014).
31. Maclaren, A., Levin, N., Lowman, H. & Trikha, M. Trph-222, a novel anti-CD22 antibody drug conjugate (ADC), has significant anti-tumor activity in NHL xenografts and is well tolerated in non-human primates. *Blood* **130**, 4105 (2017).
32. Baskin, J. M. & Bertozzi, C. R. Copper-free click chemistry: bioorthogonal reagents for tagging azides. *Aldrichimica Acta* **43**, 15–23 (2010).
33. Rockwell, S. C., Kallman, R. F. & Fajardo, L. F. Characteristics of a serially transplanted mouse mammary tumor and its tissue-culture-adapted derivative. *J. Natl Cancer Inst.* **49**, 735–749 (1972).
34. Amico, L. et al. A novel anti-HER2 anthracycline-based antibody-drug conjugate induces adaptive anti-tumor immunity and potentiates PD-1 blockade in breast cancer. *J. Immunother. Cancer* **7**, 16 (2019).
35. Wu, H. et al. Development of motavizumab, an ultra-potent antibody for the prevention of respiratory syncytial virus infection in the upper and lower respiratory tract. *J. Mol. Biol.* **368**, 652–665 (2007).
36. Kelly, R. L. et al. High throughput cross-interaction measures for human IgG1 antibodies correlate with clearance rates in mice. *MAbs* **7**, 770–777 (2015).
37. Armour, K. L., Clark, M. R., Hadley, A. G. & Williamson, L. M. Recombinant human IgG molecules lacking Fc $\gamma$  receptor I binding and monocyte triggering activities. *Eur. J. Immunol.* **29**, 2613–2624 (1999).
38. Shields, R. L. et al. High resolution mapping of the binding site on human IgG1 for Fc $\gamma$ RI, Fc $\gamma$ RII, Fc $\gamma$ RIII, and FcRn and design of IgG1 variants with improved binding to the Fc $\gamma$ R. *J. Biol. Chem.* **276**, 6591–6604 (2001).
39. Li, J. et al. Desialylation is a mechanism of Fc-independent platelet clearance and a therapeutic target in immune thrombocytopenia. *Nat. Commun.* **6**, 7737 (2015).
40. Tribulatti, M. V., Mucci, J., van Rooijen, N., Leguizamón, M. S. & Campetella, O. The trans-sialidase from *Trypanosoma cruzi* induces thrombocytopenia during acute Chagas' disease by reducing the platelet sialic acid contents. *Infect. Immun.* **73**, 201–207 (2005).
41. Assi, H., Ibrahim, S., Machiorlatti, M., Vesely, S. K. & Asch, A. S. Thrombocytopenia is a biomarker for response in patients treated with anti PD-1/PDL-1 therapy. *Blood* **132**, 1138 (2018).
42. Peng, G.-L. et al. CD8<sup>+</sup> cytotoxic and FoxP3<sup>+</sup> regulatory T lymphocytes serve as prognostic factors in breast cancer. *Am. J. Transl. Res.* **11**, 5039–5053 (2019).
43. Laoui, D. et al. Tumor-associated macrophages in breast cancer: distinct subsets, distinct functions. *Int. J. Dev. Biol.* **55**, 861–867 (2011).
44. Uchiyama, S. et al. Dual actions of group B *Streptococcus* capsular sialic acid provide resistance to platelet-mediated antimicrobial killing. *Proc. Natl Acad. Sci. USA* **116**, 7465–7470 (2019).
45. Sedlacek, H. H. & Seiler, F. R. Immunotherapy of neoplastic diseases with neuraminidase: contradictions, new aspects, and revised concepts. *Cancer Immunol. Immunother.* **5**, 153–163 (1978).
46. Barkal, A. A. et al. CD24 signalling through macrophage Siglec-10 is a target for cancer immunotherapy. *Nature* **572**, 392–396 (2019).
47. Haas, Q. et al. Siglec-9 regulates an effector memory CD8 $\beta$  T-cell subset that congregates in the melanoma tumor microenvironment. *Cancer Immunol. Res.* **7**, 707–718 (2019).
48. Jandus, C. et al. Interactions between Siglec-7/9 receptors and ligands influence NK cell-dependent tumor immunosurveillance. *J. Clin. Invest.* **124**, 1810–1820 (2014).
49. Wang, J. et al. Siglec-15 as an immune suppressor and potential target for normalization cancer immunotherapy. *Nat. Med.* **25**, 656–666 (2019).
50. Tsui, C. K. et al. CRISPR-Cas9 screens identify regulators of antibody–drug conjugate toxicity. *Nat. Chem. Biol.* **15**, 949–958 (2019).

**Publisher's note** Springer Nature remains neutral with regard to jurisdictional claims in published maps and institutional affiliations.

© The Author(s), under exclusive licence to Springer Nature America, Inc. 2020

## Methods

**Statistical analyses and reproducibility.** All statistical analyses were performed using GraphPad Prism 6, two-tailed tests were used for all *t*-tests, multiple comparisons and post hoc analyses. For one-way analysis of variance (ANOVA), *P* values of the ANOVA are reported if *P* > 0.05; if *P* < 0.05, post hoc statistics are reported (Tukey's or Dunnett's) as multiplicity-adjusted *P* values. Proteins are characterized by *n* = 1 gel and *n* = 1 mass spectrum unless otherwise noted.

**Cell lines.** SK-BR-3, ZR-75-1 and HCC-1954 were purchased from the American Type Culture Collection and cultured in filtered RPMI media 10% heat-inactivated FBS and no added antibiotics. BT-20, MDA-MB-468, MDA-MB-361, MDA-MB-231, MCF-7 and MDA-MB-453 were purchased from American Type Culture Collection and cultured in DMEM media containing 10% heat-inactivated FBS and no added antibiotics. EMT6 cells expressing the HER2 protein were a generous gift from the Zippelius laboratory (University of Basel, Switzerland) and B16D5 melanoma tumors expressing HER2, a gift from the Weiner laboratory (Lombardi Cancer Center), were cultured in DMEM supplemented with 10% FBS, 1% glutamine, 1% sodium pyruvate and 1% amino acids. Cultures were grown in T25 and T75 flasks (Thermo Fisher) and maintained at 37°C with 5% CO<sub>2</sub>. All cultures tested negative for mycoplasma infection by the Lonza MycoAlert Mycoplasma Detection Assay.

**Human NK and T cell isolation procedure.** LRS chambers were obtained from healthy anonymous blood bank donors and isolated using Ficoll-Paque (GE Healthcare Life Sciences) density gradient separation. Cells were cultured in X-VIVO 15 media (Lonza) supplemented with 5% heat-inactivated human male AB serum (Sigma-Aldrich). For some experiments, recombinant carrier-free IL-2 (Biolegend, 1:2,000 dilution) was added to further activate NK cells overnight. After 12–24 h, NK cells were isolated from peripheral blood mononuclear cells by immunomagnetic negative selection using the EasySep Human NK Cell Enrichment Kit (STEMCELL Technologies) according to the manufacturer's protocol. Human  $\gamma\delta$  T cells were isolated from peripheral blood mononuclear cells by immunomagnetic negative selection using the EasySep Human Gamma/Delta T Cell Isolation Kit (STEMCELL Technologies) according to the manufacturer's protocol.

**Detecting desialylation of cancer cells with SNA.** Cells were rinsed 1× with PBS-Ca-Mg, and lifted by incubating for ~5 min at 37°C with cell dissociation buffer (Gibco), pelleted by centrifugation 300g for 5 min, and resuspended to 1 × 10<sup>6</sup> cells per ml in normal growth media. Next, 200  $\mu$ l of cells were added to V-bottom 96-well plates (100  $\mu$ l of each cell line for mixed cell assays). Individual wells were treated with various concentrations of sialidase, conjugates or equivalent volume PBS. Cells were incubated with constructs for 1 h at 37°C, 5% CO<sub>2</sub>. Following this, cells were pelleted in the plates by centrifugation at 300g for 5 min and washed three times with PBS before staining. For SNA staining in Fig. 2, cells were resuspended in blocking buffer (PBS and 0.5% bovine serum albumin) containing Alexa Fluor 647 antihuman Her2 antibody and fluorescein isothiocyanate-labeled *S. nigra* lectin and incubated for 30 min at 4°C in the dark. Cells were then washed three times with blocking buffer and analyzed by flow cytometry on a BD Accuri C6 Plus Flow Cytometer (BD Biosciences). Flow cytometry data was analyzed using FlowJo v.10.0 software (Tree Star) and gated to distinguish HER2<sup>+</sup> and HER2<sup>-</sup> cells as well as to quantify SNA<sup>+</sup> and SNA<sup>-</sup> cells. For the flow plot in Fig. 2b, there are >16,000 cells per plot. For the analysis in Fig. 2a,c and Supplementary Fig. 4, >5,000 cells were recorded for each treatment.

**Lectin staining of HER2<sup>+</sup> EMT6 cells with biotinylated MALII/PNA.** Cells were desialylated and washed as described in the SNA protocol, then resuspended in 10  $\mu$ g ml<sup>-1</sup> of biotinylated MAL II or PNA lectin in blocking buffer, and incubated on ice for 30 min. Cells were washed three times in blocking buffer, and resuspended in Streptavidin-647 (2  $\mu$ g ml<sup>-1</sup>) in blocking buffer. After a 15-min incubation on ice, cells were washed twice more before analysis on the LSR II (BD) flow cytometer.

**Procedure for Siglec-Fc staining of cancer cells.** Breast cancer cell lines were desialylated as described before with 2  $\mu$ M ST sialidase, then resuspended in blocking buffer containing Siglec-7-Fc, -9-Fc or -F-Fc that had been pre-incubated for 30 min at 4°C with Alexa Fluor 488 AffiniPure Goat Anti-Human IgG, or Siglec-E-mFc pre-incubated for 30 min at 4°C with Alexa Fluor 647 AffiniPure Goat Anti-Mouse IgG. Cells were incubated with stain for 30 min at 4°C, followed by one wash and resuspension in blocking buffer and analysis by flow cytometry (BD Accuri C6 Plus or LSR II). Gating was performed using FlowJo software to eliminate debris (forward versus side scatter (FSC/SSC)) and analyze single cells (FSC-A/FSC-H).

**In vitro sialidase activity assays with fluorogenic 4-MUNANA.** Sialidases were diluted (10 pM–1  $\mu$ M) in Dulbecco's PBS (DPBS) containing Ca<sup>2+</sup> and Mg<sup>2+</sup> in a 96-well clear bottom black microplate (Corning 3904). Then, 2'-(4-methylumbelliferyl)- $\alpha$ -D-N-acetylneuraminic acid ('4-MUNANA', Sigma-Aldrich) was added to a 1-mM final concentration, final volume of 100  $\mu$ l. Coumarin

release was measured by fluorescence (excitation 365 nm, emission 450 nm) in the SpectraMax i3x plate reader at 37°C. Background fluorescence was subtracted from control wells lacking enzyme, and fluorescence was compared to a standard curve of 4-methylumbelliferone (0–150  $\mu$ M) (Sigma-Aldrich, M1381) to calculate the amount of hydrolyzed substrate. Specific activity (reported  $\mu$ mol substrate converted  $\times$  min<sup>-1</sup> per mg enzyme) was calculated from the rate of hydrolysis in the initial linear range (0–15 min).

**Detecting NK cell-mediated ADCC assay by lactate dehydrogenase (LDH) release.** Cells were lifted with cell dissociation buffer and resuspended in 2–5 ml of phenol red-free RPMI + 1% heat-inactivated FBS and diluted such that 1 × 10<sup>4</sup> target cells were plated in 96-well V-bottom plates (Corning), and trastuzumab, sialidase, conjugates or PBS were added to a final volume of 100  $\mu$ l and treatments were pre-incubated with target breast cancer cells for 30 min at 37°C. Next, 100  $\mu$ l of isolated effector cells in phenol red free RPMI + 1% heat-inactivated FBS were added at effector to target (E/T) ratios ranging from 0–15 for the various assays. The assay plate was incubated at 37°C + 5% CO<sub>2</sub> for 4–8 h. Cells were pelleted by centrifugation at 500g, 5 min and 50  $\mu$ l of supernatant was transferred to a 96-well flat-bottom microplate following the LDH Cytotoxicity Assay Kit (Pierce) protocol. Absorbance was measured with the SpectraMax i3x plate reader at 490 and 680 nm, final cytotoxicity was calculated according to the assay kit manufacturer's protocol.

**Detecting NK cell-mediated ADCC by flow cytometry.** Cells were lifted according with cell dissociation buffer, and resuspended in serum-free media containing 5  $\mu$ M CellTracker Green CMFDA Dye (Thermo Fisher Scientific) and incubated at 37°C for 30 min in 5% CO<sub>2</sub>. Cells were recollected by centrifugation at 300g for 5 min and resuspended in 2–5 ml normal growth media. Next, 2 × 10<sup>4</sup> cells per ml were pretreated with trastuzumab, PBS or T-Sia 2 for 30 min at a final volume of 100  $\mu$ l and human NK cells were added at an E/T ratio of 3/1. After 4 h, SYTOX Red Dead Cell Stain (Thermo Fisher Scientific) was added at 5 nM final concentration to the cell mixture, which was analyzed on the BD Accuri C6+ flow cytometer (BD Biosciences). Using FlowJo v.10.0 software (Tree Star), cells positive for CellTracker green in the FL1 channel were selected and gated for live/dead by the red FL4 channel. Data are presented with PBS-treated cells subtracted from the trastuzumab and T-Sia 2-treated mixtures (Fig. 4a).

**General DNA cloning procedures and instrumentation.** DNA gBlocks were ordered from Integrated DNA Technologies (IDT), DNA oligos were from IDT or ELIM Biopharmaceuticals. Plasmids were sequenced by ELIM Biopharmaceuticals and analyzed using SnapGene v.3.3.3. PCR was performed in the C100 Touch Thermal Cycler from Bio-Rad using the CloneAmp HiFi PCR premix (Takara). Amplified DNA was purified by 1% agarose gel in 1× TAE buffer (Bio-Rad), containing 1× SYBR Safe DNA Gel Stain (Thermo Fisher) on a Bio-Rad PowerPac HC electrophoresis power supply at 120 V, 40 min. DNA inserts were incorporated into plasmids using In-Fusion HD Enzyme premix according to the manufacturer's protocol (Takara) and transformed into Stellar Competent Cells (Takara), an *E. coli* HST08 strain and plasmid was harvested using Qiagen or Zippy plasmid miniprep kits. For bacterial sialidases, the AU54pETd<sup>+</sup> plasmid expressing *Arthrobacter ureafaciens* (AU) sialidase was a gift from S. Christensen<sup>31</sup>. pET22b-T5-A99 expressing *Clostridium perfringens* (CP) sialidase was cloned into the pET22b plasmid. pGEX-T1-Neu2 was a gift from J. Kohler and pGEX-T1-Neu3 was cloned in-house. *E. coli* C600 transformed with plasmid pCVD364 containing the VC sialidase gene was a generous gift from E.R. Vimr<sup>32</sup> (University of Illinois, Urbana-Champaign). Expression of VC was performed as previously reported<sup>22</sup>.

For mammalian expression, T-FcX antibody was cloned into Plasmid pCDNA3.1 and the isotype motavizumab antibody was cloned into the CMV/R vector<sup>33</sup> (a gift from the Kim Laboratory at Stanford). DNA for mammalian expression was isolated using the EndoFree Plasmid Maxi Kit (Qiagen). DNA sequences are in Supplementary Note 1.

**Protein characterization.** Protein concentration was determined from the absorbance at 280 nm using the NanoDrop 2000 Spectrophotometer (Thermo Fisher) and the molar extinction coefficient calculated by ExpAsy (provided by the Swiss Institute of Bioinformatics). SDS-PAGE protein gels were run on 18-well 10% Criterion XT Bis-Tris Protein Gels (Bio-Rad) at 180 V for 40–60 min. Running buffer (2×) for protein gels was made in-house and contained: 4% sodium dodecyl sulfate (Millipore Sigma), 0.004% bromophenol blue (Sigma-Aldrich), 20% glycerol (Chem-Impex) and 120 mM of Tris HCl (Sigma-Aldrich) at pH 6.8. For reduced gels, SDS-PAGE buffer additionally contained 10% 2-mercaptoethanol and gels were heated to 95°C for 5 min before gel loading. Protein gels were stained with AcquaStain Protein Gel Stain (Bulldog Bio) and imaged on a LI-COR Odyssey CLx imaging system. Protein sequences are reported in Supplementary Note 1.

**Expression and purification of antibodies.** Antibodies were expressed using the Expi293 cell expression system (Thermo Fisher Scientific) following the manufacturer's protocol. Antibodies were harvested after 7 d by collecting supernatant with brief centrifugation at 300g for 5 min followed by prolonged centrifugation to clarify the supernatant at 3,200g for 30 min at 4°C. Supernatant was then filtered through a 0.22- $\mu$ m filter unit (Fisher Scientific). Expi293

expression gave yields of  $\sim 100 \text{ mg l}^{-1}$  (trastuzumab-FcX antibody) and  $\sim 45 \text{ mg l}^{-1}$  (motavizumab). To purify, protein A-Sepharose 4B (Thermo Fisher Scientific) beads (1–3 ml) were placed in chromatography columns (Bio-Rad), washed twice with 10 ml of elution buffer (100 mM of glycine in MQ water, pH 2.8) and re-equilibrated with ( $3 \times 10 \text{ ml}^2$ ) PBS washes. After filtering transfected Expi293 supernatant, the clarified supernatant was then loaded twice. Protein A beads washed two to five times with 10 ml of PBS, and antibodies were eluted ( $2 \times 5 \text{ ml}^2$ ) into two 15 ml falcon tubes preloaded with 100  $\mu\text{l}$  of 1 M Tris buffer at pH 8 (Thermo Fisher). Antibodies were quickly buffer exchanged using PD-10 desalting columns (GE Life Sciences).

**Expression of soluble tbFGE for enzymatic aldehyde conversions.** A 5 ml culture of His6-MBP-TEV-tbFGE in BL21 (DE3) *E. coli* (New England Biolabs) in LB medium containing  $100 \mu\text{g ml}^{-1}$  ampicillin was grown overnight. After 12–16 h, two culture flasks containing 11 2xYT media (BD Diagnostic Systems) and  $100 \mu\text{g ml}^{-1}$  ampicillin were inoculated with 2 ml of the starter culture and grown at 37 °C shaking at 200 r.p.m. for 2–6 h until optical density (OD) was 0.5. The flask was cooled in ice water for 10 min, then isopropyl- $\beta$ -D-thiogalactoside (IPTG) was added to 100  $\mu\text{M}$  of final concentration, culture was shaken at 250 r.p.m. at 18 °C overnight. After 20 h, the bacterial pellets were collected at 6,000g for 20 min and frozen at  $-80^\circ\text{C}$ . Bacterial pellets were resuspended in 100 ml of lysis buffer (1 $\times$  DPBS-Ca, -Mg, 150 mM of NaCl, 10 mM of imidazole, 1 mM of TCEP, pH 7.5) and two protease inhibitor tablets (Roche) and 10  $\mu\text{l}$  of Pierce nuclease (0.1  $\mu\text{l ml}^{-1}$ ) (Thermo Fisher). Pellet suspension was shaken at 150 r.p.m. for 2 h at 4 °C. Cell lysis was accomplished by three passes through an EmulsiFlex-C3 homogenizer (Avestin) at 15 kPa, followed by centrifugation at 13,000g for 30 min. When lysed bacteria were finished centrifuging, supernatant was collected and equilibrated nickel resin (Thermo Fisher) was added, 3 ml per liter of original culture. Resin was incubated at 4 °C for 30 min, loaded onto a chromatography column, washed with 900 ml of washing buffer (1 $\times$  DPBS-Ca, -Mg, 150 mM of NaCl, 20 mM of imidazole, 1 mM of TCEP, pH 7.5) and eluted with 10 ml of elution buffer (1 $\times$  DPBS-Ca, -Mg, 150 mM of NaCl, 250 mM of imidazole, 1 mM of TCEP, pH 7.5). Elution was concentrated with a 10,000 molecular weight cut-off Amicon filter (Millipore Sigma, UFC901024) and buffer exchanged into TEAM buffer (25 mM of TEA, 50 mM of NaCl, pH 9) plus 2 mM of  $\beta$ -mercaptoethanol (BME). Glycerol was added to a final concentration of 10% and tbFGE was flash-frozen in liquid nitrogen and stored as aliquots at  $-80^\circ\text{C}$ ; final yield was  $15 \text{ mg l}^{-1}$ .

**Representative expression and purification of sialidase with His-tag.** A 5-ml culture of N-His-ST Sialidase-C-Aldehyde tag in pET151 plasmid transformed into BL21 (DE3) *E. coli* (New England Biolabs) was inoculated from a glycerol stock and grown overnight at 37 °C with shaking at 200 r.p.m. in LB medium containing  $100 \mu\text{g ml}^{-1}$  of ampicillin (Sigma-Aldrich). The following day, 3 l of Difco 2xYT media (BD Diagnostic Systems) containing  $100 \mu\text{g ml}^{-1}$  of ampicillin were inoculated with the overnight culture. Cells were grown at 37 °C with shaking at 200 r.p.m. for 4 h until the OD was 0.6, then IPTG was added (0.3 mM final concentration). Cells were induced for 16 h at 27 °C, with shaking at 250 r.p.m. Cultures were pelleted by centrifugation at 5,100g for 40 min, and pellet was frozen overnight at  $-80^\circ\text{C}$ . The next day, pellet was thawed for homogenization and nickel column purification as described before for tbFGE except with a different lysis buffer (PBS + 150 mM of NaCl and 10 mM of imidazole, pH 7.3), wash buffer (PBS + 150 mM of NaCl and 20 mM of imidazole, pH 7.3) and elution buffer (PBS + 150 mM of NaCl and 250 mM of imidazole, pH 7.3). Purified protein was run four times through endotoxin-removal resin (Thermo Fisher) followed by buffer exchange using a PD-10 column. The final yield was  $\sim 18 \text{ mg}$  per liter of bacterial culture. *C. perfringens* and *A. ureafaciens* sialidases were purified identically, except that kanamycin was used as a selection marker for the AU54pET9d\* plasmid.

**Procedure for glutathione S-transferase (GST) purification of Neu2 and Neu3 proteins.** pGEX-T1-Neu2/Neu3 plasmids were transformed into BL21 (DE3) *E. coli* (New England Biolabs C25271). Cells were grown in 2xYT media, supplemented with ampicillin ( $100 \mu\text{g ml}^{-1}$ ), at 37 °C with shaking at 200 r.p.m. overnight. The following day, a 1-l culture of 2xYT broth containing ampicillin was inoculated from the overnight stock and grown for 3 h until OD was 0.6. Protein production was induced with 0.1 mM of IPTG and cells were incubated at 30 °C with shaking at 200 r.p.m. for 16 h. The next day, cell pellets were collected by centrifugation at 5,000g for 15 min. Cells were lysed in GST binding buffer (50 mM of Tris-Cl (pH 8), 150 mM of NaCl and 0.1 mM of EDTA), with a dounce homogenizer followed by running three times through an EmulsiFlex-C3 homogenizer. Clarified lysate was isolated by centrifugation at 13,000g for 40 min. Meanwhile the GST column was prepared by adding 0.5 ml of glutathione sepharose beads (Sigma) to a column, and washing with 10 column volumes (CV) of elution buffer (50 mM of Tris-Cl pH 8, 150 mM of NaCl, 0.1 mM of EDTA and 10 mM of freshly prepared reduced glutathione (Sigma)), followed by 30 CV of GST binding buffer. Clarified lysate was added to the prepared column, and beads were suspended by mixing. Beads were mixed with lysate for 30 min at room temperature on a rocker. The column was placed on a stand and beads were allowed to settle. The column was washed with GST binding buffer until no protein

was detected in the flow through as monitored by the Quick Start Bradford kit (Bio-Rad, 500-0202). Then, 0.5 CV GST Elution buffer was added to the beads and immediately eluted to make the first elution fraction. This was followed by a 10-min incubation with 0.5 CV of GST elution buffer on the beads before eluting to yield elution fraction 2. Beads were then washed with a further 1–5 CV of GST Elution buffer and fractions were collected. Elution fractions were analyzed by SDS-PAGE and the purest fractions were collected to yield of roughly 2 mg of protein per 1 l of culture.

**Copper-click reaction for fluorophore labeling of antibodies.** To azide-labeled antibody (265.5  $\mu\text{l}$ , 14  $\mu\text{M}$ ) in PBS was added Alexa Fluor 647-alkyne (3  $\mu\text{l}$ , 100  $\mu\text{M}$ , from 10 mM of dimethylsulfoxide (DMSO) stock). A premixed solution of 20 mM  $\text{CuSO}_4$  + 100 mM of BTAA ligand in water was added to the reaction (1.5  $\mu\text{l}$ , 0.1 mM of  $\text{CuSO}_4$ , 0.5 mM of BTAA). This was quickly followed by aminoguanidine (15  $\mu\text{l}$ , 5 mM, from 100 mM of PBS stock), and freshly dissolved sodium ascorbate (15  $\mu\text{l}$ , 5 mM, from 100 mM of PBS stock). The reactions were rotated slowly at room temperature, 1 h under argon. EDTA was added (1  $\mu\text{l}$ , 1.67 mM) to quench the copper, and proteins were buffer exchanged into PBS by repeated centrifugations and PBS washes in an Amicon Ultra-0.5-ml 50-kDa cut-off centrifugal filter unit (EMD Millipore). Equivalent conjugation to make the antibody-fluorophore conjugates trastuzumab-oxime-AF647 and trastuzumab-HIPS-AF647 was confirmed by absorbance at 280- and 650-nm wavelengths using the NanoDrop 2000 Spectrophotometer.

**Representative procedure for fGly conversion.** TbFGE in TEAM buffer (25 mM of triethanolamine, 50 mM of NaCl, pH 9) (101.4  $\mu\text{l}$ , final 0.9  $\mu\text{M}$ , 0.1 equiv.) was added to Motavizumab in TEAM buffer (3.7 ml, final 9  $\mu\text{M}$ , 1 equiv.) and  $\text{CuSO}_4$  (5 mM stock in MQ water) was immediately added to 5  $\mu\text{M}$  final concentration. 2-Mercaptoethanol was added for a final concentration of 2 mM. Conversion occurred at 37 °C, 400 r.p.m. for 16 h and was analyzed by electrospray ionization-time-of-flight mass spectrometry. Antibodies were repurified by protein A chromatography as described before.

**Representative procedure for HIPS-azide addition to antibody.** Trastuzumab fGly was buffer exchanged by PD-10 column into 50 mM of sodium citrate and 50 mM of NaCl, pH 5.5. HIPS-azide (Supplementary Note 2) was dissolved in DMSO to 36 mM, and added (11.987  $\mu\text{mol}$ , 20 equiv., 333  $\mu\text{l}$ ) to trastuzumab fGly in citrate buffer (600.6 nmol, 1 equiv., 7.947 ml). The mixture was shaken at 230 r.p.m. and 37 °C overnight, followed by PD-10 buffer exchange into PBS. Only HIPS-converted trastuzumab was detected, with an apparent 96% recovery of protein.

**Procedure for  $\alpha$ -chloroacetamide labeling of ST sialidase.** ST sialidase (1.04  $\mu\text{mol}$ , 1 equiv., 16 ml) in 50 mM ammonium bicarbonate buffer pH 8.3 was incubated in the dark with TCEP (2 mM final concentration, 66  $\mu\text{l}$ ), while shaking at 300 r.p.m. for 10 min.  $\alpha$ -chloroacetamide-DBCO (Supplementary Note 2) was dissolved into DMSO to 50 mM and added to the ST sialidase solution (20.88  $\mu\text{mol}$ , 20 equiv., 417.6  $\mu\text{l}$ ), and the mixture was shaken in the dark at 300 r.p.m. overnight at room temperature in a 50-ml falcon tube. Reaction completion was monitored by ultraviolet-visible lights measurements at 280 and 309 nm to check for the percentage of conjugated DBCO. Once fully conjugated, purification was performed using a HiLoad 26/600 Superdex 75pg on the ÄKTA pure chromatography system in PBS at 4 °C, followed by 0.2- $\mu\text{m}$  syringe filtration.

**Maleimide-PEG4-DBCO labeling of ST sialidase.** To ST sialidase (618 nmol, 30 ml, 1 equiv.) in PBS, TCEP was added (30  $\mu\text{mol}$ , 60  $\mu\text{l}$ ) (Fisher Scientific) and the mixture was rotated at 4 °C for 30 min protected from light. Maleimide-PEG4-DBCO (12.36  $\mu\text{mol}$ , 20 equiv., 618  $\mu\text{l}$ ) (Click Chemistry Tools) in DMSO was added and the reaction was mixed at 600 r.p.m. for 2.5 d at 4 °C. Purification was performed using a HiLoad 26/600 Superdex 75pg on the ÄKTA pure chromatography system in PBS.

**Representative synthesis of antibody-sialidase conjugate.** T-FcX-HIPS-azide (63.3 nmol, 1 equiv., 11.9 ml) and ST sialidase (316.9 nmol, 5 equiv., 16 ml), both in PBS buffer, were mixed together and concentrated to  $\sim 25 \text{ mg ml}^{-1}$  using 10,000 molecular weight cut-off Amicon spin filters. The final mixture ( $\sim 0.92 \text{ ml}$ ) was incubated at 25 °C in the dark with shaking at 500 r.p.m. for 3 d. The reaction was monitored by SDS-PAGE and purified by size exclusion chromatography using a Superdex 200 increase 10/300 column on the ÄKTA pure chromatography system in PBS (GE Healthcare Life Sciences), followed by protein A chromatography. Final conjugates were buffer exchanged to PBS buffer with PD-10 columns and 0.2- $\mu\text{m}$  was syringe filtered.

**Endotoxin detection.** The HEK-Blue LPS Detection Kit (Invivogen, rep-lps2) was used according to the manufacturer's protocol. Briefly, serial dilutions of antibody-enzyme conjugates were incubated with HEK-Blue cells both alone and spiked with 0.1 EU  $\text{ml}^{-1}$  of endotoxin standard to verify that no inhibition occurred. After 24 h, an aliquot of the cell media was incubated with QUANTI-Blue reagent (Invivogen), absorbance was read on a SpectraMax i3x Multi-Mode microplate reader and

then compared to a standard curve. For all *in vitro* cell experiments and mouse experiments, endotoxin of the antibody–enzyme conjugates was determined to be  $<1$  EU  $\text{mg}^{-1}$ .

**Determining  $K_D$  of T-Sia 2.** HER2<sup>+</sup> HCC-1954 cells were lifted with cell dissociation buffer, pelleted with centrifugation and resuspended to  $1 \times 10^6$  cells per ml in PBS and 0.5% BSA, and 180  $\mu\text{l}$  were distributed into wells of a 96-well V-bottom plate (Corning). Various concentrations (20–0.01 nM) of trastuzumab or T-Sia 2 were added to the cells in equal volumes and incubated with cells for 30 min at 4°C. Following this, cells were washed three times in blocking buffer, pelleting by centrifugation at 300g for 5 min between washes. Cells were resuspended in Alexa Fluor 488 AffiniPure Goat Anti-Human IgG in blocking buffer for 15 min at 4°C. Cells were further washed twice and resuspended in blocking buffer, and fluorescence was analyzed by flow cytometry (BD Accuri C6 Plus). Gating was performed using FlowJo v.10.0 software (Tree Star) to eliminate debris and isolate single cells. Median fluorescence intensity of the cell populations were subtracted from control cells treated with secondary antibody only, and normalized to the maximum median fluorescence intensity population from each experimental replicate. Values were fit to a one-site total binding curve using GraphPad Prism 6, which calculated the  $K_D$  values as the antibody concentration needed to achieve a half-maximum binding.

**Biolayer interferometry binding experiments.** Reactions were run on an Octet Red 96 and samples were run in PBS with 0.1% BSA and 0.05% Tween (PBST BSA), except in the case of mouse FcRn binding, where reactions were run in PBST BSA with the pH adjusted to 6. Mouse Fc receptors were loaded onto streptavidin (SA) biosensors (ForteBio) and the load threshold was set to 0.5 nm (or 2 nm for FcRn). After loading, the tips were washed and then were associated in 100 nM of each antibody in PBST BSA (or PBST BSA pH 6 for FcRn) for 0.333 min and dissociated for 0.666 min. All samples were baseline subtracted to a well that loaded the tip with Fc receptor but did not go into the antibody as a control for any buffer trends within the samples. The resulting binding curves were fit in GraphPad Prism.

**Plasma stability assay of HIPS linker.** Antibody–fluorophore conjugates were added to 80% human plasma at daily intervals and kept at 37°C (final 0.56  $\text{mg ml}^{-1}$  concentrations of antibodies in 80% plasma). On day 4, aliquots were diluted 1:193 in PBS and incubated on the surface of lifted HCC-1954 cells in blocking buffer for 30 min on ice, followed by flow cytometry to detect conjugated fluorophore. Quantification was performed by comparing to a standard curve of cells incubated with antibody–fluorophores at 20, 10, 5, 1 and 0.1 nM.

**Stability of HIPS linker on cells.** Trastuzumab–oxime–647 and trastuzumab–HIPS–647 were assessed for their stability on HER2<sup>+</sup> HCC-1954 cells. Briefly, HCC-1954 cells were plated at high confluence ( $4 \times 10^4$  cells per well) on a black-walled, clear-bottomed 96-well plate (Corning) and allowed to adhere for 24 h in normal growth conditions. In some experiments, cells were then fixed by washing twice with PBS containing  $\text{Ca}^{2+}$  and  $\text{Mg}^{2+}$ , followed by 15 min in 4% PFA at room temperature and three PBS washes. Antibody–fluorophores (50 nM) were then added in phenol red-free RPMI buffer (100  $\mu\text{l}$  per well) and incubated for 30 min 37°C, 5%  $\text{CO}_2$ . Then free antibodies were removed and replaced with phenol red-free RPMI. In some experiments, 100  $\mu\text{M}$  of leupeptin (EMD Millipore) protease inhibitor was included in the media. Fluorescence was monitored in an InCyte S3 Live Cell Analysis System (Sartorius) within a Thermo Fisher Scientific tissue culture incubator at 37°C with 5%  $\text{CO}_2$ . Data were acquired using a  $\times 10$  objective lens in phase contrast, and red fluorescence (ex.  $585 \pm 20$ , em.  $665 \pm 40$ ; acquisition time, 800 ms) channels. Images (1,392  $\times$  1,040 pixels at 1.22  $\mu\text{m}$  per pixel) were acquired from each well at 2-h intervals. The quantification of red fluorescence on live cells was analyzed with the following settings: Top-Hat segmentation with a 100- $\mu\text{m}$  radius and threshold adjustment: 0.2; edge split on; edge sensitivity –25; hole fill 200  $\mu\text{m}^2$ ; filter area maximum 2,600  $\mu\text{m}^2$  and mean intensity maximum 2.4  $\mu\text{m}^2$ . For fixed cells the analysis was: Top-Hat segmentation with 100- $\mu\text{m}$  radius and threshold adjustment: 0.3; edge split on; edge sensitivity –35 and hole fill 0  $\mu\text{m}^2$ . The total red object integrated intensity (RCU  $\times \mu\text{m}^2$  per image) from PBS-treated samples was subtracted from the integrated intensity of the antibody–fluorophore wells and is reported as integrated fluorescence intensity.

**Trypsin digest and mass spectrometry of digested proteins.** Reduction and alkylation were performed according to ProteaseMax (Promega) protocols. Briefly, samples (5  $\mu\text{g}$ ) were diluted to 93.5  $\mu\text{l}$  with 50 mM of ammonium bicarbonate. Then, 1  $\mu\text{l}$  of 0.5 M DTT was added and the samples were incubated at 56°C for 20 min, followed by the addition of 2.7  $\mu\text{l}$  of 0.55 M iodoacetamide at room temperature for 15 min in the dark. Digestion was completed by adding sequencing-grade trypsin (Promega) in a 1:20 enzyme to protein ratio overnight at 37°C, and quenched by adding 0.3  $\mu\text{l}$  of glacial acetic acid. C18 clean-up was performed using SPEC tips (Agilent). Each tip was wetted with 200  $\mu\text{l}$  of methanol three times, followed by three 200- $\mu\text{l}$  rinses of buffer A (5% formic acid in water). The samples were diluted to 200  $\mu\text{l}$  in buffer A and loaded through the column 5–6 times, then rinsed three times with buffer A. Finally, the

samples were eluted with three rinses of 100  $\mu\text{l}$  of buffer B (5% formic acid, 80% acetonitrile) and dried by speedvac.

Samples were reconstituted in 10  $\mu\text{l}$  of 0.1% formic acid (Thermo Fisher Scientific) and were analyzed by online nanoflow liquid chromatography–tandem MS using an Orbitrap Fusion Tribrid mass spectrometer (Thermo Fisher Scientific) coupled to a Dionex Ultimate 3000 HPLC system (Thermo Fisher Scientific). A portion of the sample (4  $\mu\text{l}$ ) was loaded via autosampler onto a 20- $\mu\text{l}$  sample loop and injected at 0.3  $\mu\text{l min}^{-1}$  onto a 75- $\mu\text{m} \times 250$ -mm EASY-Spray column (Thermo Fisher Scientific) containing 2  $\mu\text{m}$  C18 beads. The column was held at 40°C using a column heater in the EASY-Spray ionization source (Thermo Fisher Scientific). The samples were eluted at 0.3  $\mu\text{l min}^{-1}$  using a 90-min gradient and a 185-min instrument method. Solvent A was composed of 0.1% formic acid in water, whereas solvent B was 0.1% formic acid in acetonitrile. The gradient profile was as follows (min/%B): 0:3, 3:3, 93:35, 103:42, 104:98, 109:98, 110:3 and 185:3. The instrument method used an MS1 resolution of 60,000 at a full-width at half-maximum of 400  $m/z$ , an automatic gain control target of  $3 \times 10^5$  and a mass range from 300 to 1,500  $m/z$ . Dynamic exclusion was enabled with a repeat count of three, repeat duration of 10 s and exclusion duration of 10 s. Only charge states 2–6 were selected for fragmentation. MS2 resolutions were generated at top speed for 3 s. HCD was performed on all selected precursor masses with the following parameters: isolation window of 2  $m/z$ , 28–30% collision energy, orbitrap (resolution of 30,000) detection and atomic gain control target of  $1 \times 10^4$  ions. All cysteine-containing peptides were manually sequenced using Xcalibur software and confirmed the presence of carbidomethyl (+57), DBCO (+774) or reduced DBCO (+563). Extracted ion chromatograms were used to calculate relative abundance of the peptides for estimation of reaction efficiency.

**Reversed-phase–high-performance liquid chromatography (RP–HPLC).** Antibody conjugates (1  $\text{mg ml}^{-1}$ ) were buffer exchanged into 100 mM of ammonium bicarbonate and 8 M of urea in water (pH 8.3). DTT was added to 5 mM of the final concentration and the antibody was heated to 56°C, with shaking at 700 r.p.m. for 25–45 min in an Eppendorf thermomixer. The sample was allowed to cool and 14 mM of iodoacetamide was added from a freshly prepared 500 mM of stock in water; the sample was protected from light and incubated at 25°C with shaking at 700 r.p.m. for 30 min. The reaction was quenched by addition of another 5 mM of DTT and incubated again in the dark, at room temperature, 700 r.p.m. for 15 min. RP–HPLC was performed on a 1100/1200 series instrument (Agilent Technologies) connected in-line to a ultraviolet-visible light spectrophotometer. A total of 10  $\mu\text{g}$  of protein was injected onto a Zorbax 3.5- $\mu\text{m}$  300SB 300 Å C8 2.1  $\times$  50-mm column (Agilent). RP–HPLC was performed at 0.9  $\text{ml min}^{-1}$  at 60°C using 0.1% trifluoroacetic acid (TFA) in water (mobile phase A, MPA) and 0.1% TFA in acetonitrile (mobile phase B, MPB). The 28-min method consisted of a 4 min isocratic hold at 28% MPB, a linear gradient for 6 min to 34% MPB, an isocratic hold at 34% MPB for 1.5 min to increase the separation between heavy chain (HC) and HC–Sia and a 6.5-min linear gradient to 42% MPB, followed by a 5 min wash using 100% MPB and a 5 min re-equilibration at 28% MPB. Antibody to enzyme ratio (EAR) was calculated by integrating the area-under-the-curve of the light chain and HC peaks, and calculating molar ratios of the antibody chains using the protein extinction coefficients at 280 nm. When HC and HC–Sia were not perfectly separated, as in the case of motavizumab, the ratio of light chain moles to heavy chain (conjugated or free) moles was assumed to be 1, and the combined area under the curve of the heavy chains were used to determine the EAR.

**Mass spectrometry of full-length proteins.** Protein samples (30  $\mu\text{l}$ ,  $\sim 10 \mu\text{M}$ ) in PBS or 50 mM of ammonium bicarbonate buffer were treated with 1  $\mu\text{l}$  of PNGaseF (New England Biolabs) overnight at 37°C. Following this, the samples were analyzed by electrospray ionization–liquid chromatography mass spectrometry on an Agilent 1260 HPLC and Bruker MicroTOF-Q II time-of-flight mass spectrometer. The column was a Waters BioResolve RP mAb Polyphenyl 450A 2.7  $\times$  100  $\times$  2.1 mm maintained at 50°C; the flow rate was 0.3  $\text{ml min}^{-1}$  and the injection volume was 5  $\mu\text{l}$ . Solvent A was 0.095% formic acid and 0.05% TFA in water, solvent B was 0.1% formic acid in acetonitrile. The gradient began with 5% B held for 1.5 min then ramped to 35% B at 2 min, 46% B at 10 min and 95% B at 11 min held for 1 min. Data was collected in full scan MS mode with a mass range of 400–4,000 Da with a Collision RF setting of 800 V. The protocol for trypsin digest and mass spectrometry of digested proteins is detailed in the Supplemental methods

**T-Sia 2 treatment of EMT6 tumors in mice.** All tumor growth mouse experiments were performed in Basel, followed all relevant ethical regulations and were approved by the local Ethical Committee (Basel Stadt). BALB/c mice were obtained from Janvier Laboratories (France) and bred in-house at the University Hospital Basel, Switzerland. Animals were housed under specific pathogen-free conditions. For tumor growth experiments, 7–9-week-old females were used. EMT6-HER2 cells were injected into the right mammary fat pad of female BALB/c mice ( $1 \times 10^6$  cells in 40  $\mu\text{l}$  of PBS). All treatments were given *i.p.* by a blinded experimenter. A total of four doses were administered every second to third day once the tumor size reached approximately 100  $\text{mm}^3$ . Tumor size and health score, as well as weight, were measured and monitored three times weekly by an individual blinded to

the treatment groups. Perpendicular tumor diameters were measured by caliper and tumor volume calculated according to the following formula: tumor volume ( $\text{mm}^3$ ) =  $(d^2 \times D)/2$ , where  $d$  and  $D$  are the shortest and longest diameters of the tumor (in millimeters), respectively. Mice were killed once tumor size reached approximately  $1,500 \text{ mm}^3$  (tumor growth experiment in Fig. 4) or  $1,000 \text{ mm}^3$  (tumor growth experiment in Fig. 5) or when the mice presented ulceration (that required euthanasia within 24 h according to local law). All animals injected with conjugates were included in the survival analyses; however, ulcerated tumors were excluded from further TIL or glycosylation analysis for the sake of homogeneity.

**Leukocyte analysis.** For analysis of tumor-infiltrating immune cells, resected tumors gathered at the survival endpoints of experiments were mechanically dissociated and digested with a mixture of Accutase, collagenase IV, hyaluronidase and DNase type IV. Samples were filtered through a  $70\text{-}\mu\text{m}$  mesh and tumor-infiltrating lymphocytes were enriched by density centrifugation using Histopaque-1119 (Sigma). Samples were frozen (90% FCS, 10% DMSO) and stored in liquid nitrogen until further analysis. Multicolor flow cytometry was performed on single cell suspensions. Samples were incubated with fixable live/dead dye and Fc receptor block followed by staining with primary antibodies. Stained samples were fixed with IC fixation buffer (eBioscience) until time of analysis. For intracellular staining, samples were permeabilized after fixation. All tumor samples were analyzed by flow cytometry using a Fortessa LSR II flow cytometer (BD Biosciences) and cells analyzed after serial duplet exclusion and live/dead discrimination using FlowJo v.10.0 software (Tree Star).

**Glycosylation analysis and localization of T-Sia 2 in mice.** T-Sia 2 imaging studies on mice were performed at Stanford, and their care monitored by the Veterinary Service Center at Stanford University under APLAC protocol no. 31511 and was compliant with all relevant ethical regulations. T-Sia 2 was labeled with 3 equiv. IRDye 800CW NHS ester at pH 8.3 in PBS for 1 h. Unconjugated dye was removed, and conjugate was buffer exchanged into PBS using 7 MWCO Zeba Spin Desalting Columns (Thermo Scientific). Fluorophore labeling was quantified by nanodrop ultraviolet-visible measurements at 280 and 774 nm and diluted to a 1:1 fluorophore:conjugate ratio using unlabeled T-Sia 2. Balb/c mice (BALB/cAnNCrCl, Charles River, 7–9-week-old females) were then injected s.c. with  $1 \times 10^6$  HER2<sup>+</sup> EMT6 cells in  $100 \mu\text{l}$  of PBS. After 5 d (Fig. 4e), mice were injected i.p. with fluorophore-labeled T-Sia 2. Live mice were anesthetized with isoflurane and imaged at 2 and 4 d on an IVIS Lumina instrument (ex. 700 nm, em: 790 nm, 2 s exposure time). Four days after conjugate injection, mice were killed and organs and tumors were re-imaged by IVIS ex vivo. Tumors were then either resuspended and stained for lectin staining by flow cytometry, or frozen for histology as described next. These scientists were not blinded for these experiments. For the glycosylation analysis in Fig. 5c, mice were injected with HER2<sup>+</sup> EMT6 as described before, but treatment of 20 pmol of T-Sia 2 or Isotype-Sia was injected i.p. after 11 d to allow for larger tumor size and cell counts by flow cytometry. Four days after conjugate injection, mice were killed and tumors were resuspended for flow cytometry described next.

**Lectin staining of mouse tumor suspensions.** Resected tumors were mechanically dissociated and digested with a mixture of Accutase, collagenase IV, hyaluronidase and DNase type IV. Samples were filtered through a  $70\text{-}\mu\text{m}$  mesh filter. Lectin staining was performed using biotinylated PNA, SNA, MALII and ConA obtained from Vector Laboratories. Single cell suspensions of tumor digests were incubated with lectins at  $10 \mu\text{g ml}^{-1}$  and detected in a second step using  $2 \mu\text{g ml}^{-1}$  Streptavidin-PE-Cy7 (Extended Data Fig. 4c, experiments done in Basel) or Streptavidin-AF647 (Fig. 5c and Extended Data Fig. 5e, experiments done at Stanford) for 20 min at 4°C. Sialylation was assessed by flow cytometry using a CytoFLEX (Beckman Coulter) cytometer or an LSR II (BD) and quantified after live/dead and duplet exclusion using the geometric mean of lectin staining. ConA was used as a sialic acid-independent control for the samples prepared in Basel examining long-term desialylation taken over different time points; for the short-term desialylation experiments performed at Stanford, ConA staining was not performed.

**Fluorescence microscopy on mouse tissues.** Tissues were rapidly frozen in blocks of OCT compound on dry ice. Tissue slices were cut into  $8\text{-}\mu\text{m}$  slices using a cryostat at  $-20^\circ\text{C}$  (Leica), and placed on microscope slides (Thermo) that were stored at  $-80^\circ\text{C}$ . Positive control slides were incubated with  $6 \mu\text{M}$  of ST sialidase and  $600 \text{ nM}$  of VC sialidase at  $37^\circ\text{C}$  for 30 min. Then all slides were washed once in PBS and fixed in ice-cold methanol for 10 min, followed by three washes in PBS. Cells were blocked for 30 min in carbohydrate-free blocking buffer (Vector Laboratories) containing streptavidin (Vector), followed by 10 min with biotin (Vector Laboratories) in carbohydrate-free blocking buffer. Slides were rinsed three times in PBS and stained with lectin ( $20 \mu\text{g ml}^{-1}$ ) MAL II, SNA or PNA, (Vector Laboratories) for 1 h at room temperature in carbohydrate-free blocking buffer followed by three washes in PBS, 5 min each. Slides were then stained with  $15 \mu\text{g ml}^{-1}$  of Alexa Fluor 647-conjugated Streptavidin-647 (Thermo) for 30 min at room temperature in the dark. After three further PBS washes, slides were mounted (ProLong Gold Antifade Mountant with 4,6-diamidino-2-phenylindole, Thermo) and placed under a coverslip. Imaging of tissue samples was performed

on an Axio Observer Z-1 (Zeiss) equipped with a Spectra-X Light engine LED light (Lumencor), controlled with Micro-Manager. Images were acquired with a Plan-Apochromat  $\times 20/0.8$  air objective (Zeiss) paired with image capture from the ORCA-Flash4.0 sCMOS camera (sCMOS; Hamamatsu) AF657 was excited with a 631-nm light (LED; 631 nm, 28-nm bandpass) with an LED power of 100%. Emission from AF647 was collected with a 680/10-nm bandpass emission filter after passing through a dichroic mirror (425/30, 514/30, 592/25, 709/100 nm Longpass filter).

**Sig-E<sup>-/-</sup> mouse experiments.** All tumor-growth mouse experiments were performed in Basel and approved by the local Ethical Committee (Basel Stadt) and complied with ethical regulations. Male and female C57BL/6 WT and Siglec-E deficient mice (Sig-E<sup>-/-</sup>), 10–12 weeks old were used to perform experiments in Fig. 6. The Siglec-E deficient mouse was provided by A. Varki (UCSD)<sup>44</sup> and the mice were bred and backcrossed to the local C57BL/6 strain in-house at the University Hospital, Basel, in heterozygous breedings for more than nine generations. The scientist was not blinded for these experiments. Briefly, 500,000 HER2<sup>+</sup> B16D5 cells in  $200 \mu\text{l}$  PBS were injected s.c. into the flanks of WT or Sig-E<sup>-/-</sup> mice. Tumor growth and mice scores were measured three times per week until death on ulceration or when reaching the maximum size of  $\sim 1,500 \text{ mm}^3$ . Treatment began 7 d after the tumor cells were injected; antibody conjugates were injected every 2 d i.p. ( $10 \text{ mg kg}^{-1}$ ), for a total of four injections. Results were compiled from independently performed mouse experiments shown in Extended Data Fig. 9. For analysis of Siglec-E expression in tumor-infiltrating leukocytes, tumors were harvested on mouse death and frozen until flow cytometry was performed as described before. The percentage of Siglec-E<sup>+</sup> cells were quantified by flow cytometry gating in Supplementary Fig. 22 and fluorescence-minus one controls were subtracted. The mean background percentage of Siglec-E<sup>+</sup> in the Sig-E<sup>-/-</sup> control group was quantified and subtracted from the percentage of Siglec-E<sup>+</sup> of WT mice.

**Blood counts.** Blood was collected from the tail vein of PBS, trastuzumab and T-Sia 2-treated mice (Fig. 5) into EDTA-coated Microtainers (BD Biosciences) 48 h after the first dose of treatment. Generally,  $40\text{--}60 \mu\text{l}$  of blood were diluted to total volume of  $240 \mu\text{l}$  using 0.9% NaCl. Complete blood counts were measured on the ADVIA120 Hematology Analyzer using the Multispecies v.5.9.0-MS software (Bayer) and adjusted to the respective dilution factor.

**Reporting Summary.** Further information on research design is available in the Nature Research Reporting Summary linked to this article.

## Data availability

All data shown in this manuscript are provided either as source data files or in Supplementary Dataset 1. Any unique materials presented in the manuscript may be available from the authors upon reasonable request and through a materials transfer agreement.

## References

- Christensen, S. & Egebjerg, J. Cloning, expression and characterization of a sialidase gene from *Arthrobacter ureafaciens*. *Biotechnol. Appl. Biochem.* **41**, 225–231 (2005).
- Vimr, E. R., Lawrisuk, L., Galen, J. & Kaper, J. B. Cloning and expression of the *Vibrio cholerae* neuraminidase gene nanH in *Escherichia coli*. *J. Bacteriol.* **170**, 1495–1504 (1988).
- Barouch, D. H. et al. A human T-cell leukemia virus type 1 regulatory element enhances the immunogenicity of human immunodeficiency virus type 1 DNA vaccines in mice and nonhuman primates. *J. Virol.* **79**, 8828–8834 (2005).
- Angata, T., Nycholat, C. M. & Macauley, M. S. Therapeutic targeting of Siglecs using antibody- and glycan-based approaches. *Trends Pharmacol. Sci.* **36**, 645–660 (2015).
- Ikehara, Y., Ikehara, S. K. & Paulson, J. C. Negative regulation of T cell receptor signaling by Siglec-7 (p70/AIRM) and Siglec-9. *J. Biol. Chem.* **279**, 43117–43125 (2004).
- Crespo, H. J., Lau, J. T. Y. & Videira, P. A. Dendritic cells: a spot on sialic acid. *Front. Immunol.* **4**, 491 (2013).
- Munday, J., Floyd, H. & Crocker, P. R. Sialic acid binding receptors (Siglecs) expressed by macrophages. *J. Leukoc. Biol.* **66**, 705–711 (1999).
- von Gunten, S. & Bochner, B. S. Basic and clinical immunology of Siglecs. *Ann. NY Acad. Sci.* **1143**, 61–82 (2008).
- Nguyen, K. A. et al. Role of Siglec-7 in apoptosis in human platelets. *PLoS ONE* **9**, e106239 (2014).
- Toubai, T. et al. Siglec-G represses DAMP-mediated effects on T cells. *JCI insight* **2**, e92293 (2017).

## Acknowledgements

We thank S. Banik, C.J. Cambier and S. Wisnovsky for critical reading of this manuscript, T. McLaughlin and the Stanford University Mass Spectrometry facility for intact protein

characterization and high-resolution mass spectrometry analysis and the Stanford Shared FACS Facility for use of flow cytometry instruments. We are grateful to A. Zippelius (University of Basel) for providing the HER2<sup>+</sup> EMT6 cell line, D. Rabuka (Catalent Pharma Solutions) for providing SMARTag trastuzumab, M. Appel (Stanford University) for generating the pET28-MBP-tev-tb-FGE plasmid, as well as C.C. Angelakos for assistance with and usage of the Leica cryostat. We thank S. Christensen (University of Copenhagen) for the AU54pET9d<sup>+</sup> plasmid, E. Vimr (University of Illinois Urbana-Champaign) for the plasmid pCVD364 and J. Kohler (UT Southwestern) for the pGEX-Neu2 construct. This work was supported in part by the Goldschmidt-Jacobson Foundation (H.L.), the Promedica Foundation (M.A.S) and a Swiss National Science Foundation grant (no. 310030\_184720/1) (H.L.), as well as a grant from the National Institutes of Health (no. NIH CA227942 to C.R.B.) Researchers were also supported by the National Science Foundation Graduate Research Fellowship (M.A.G., G.A. and P.A.W.) and the Stanford ChEM-H Chemistry/Biology Interface Predoctoral Training Program (M.A.G. and P.A.W.) as well as the Swiss Government Excellence Scholarship for Foreign Scholars and Artists (N.R.M.), the Conselho Nacional de Desenvolvimento Científico e Tecnológico (N.R.M.), an NIH F32 Postdoctoral Fellowship (S.A.M.), the Stanford Undergraduate Summer Research Program in Chemistry funded through Stanford VPUE/UAR (J.T.T.) and the US National Institutes of Health Predoctoral Fellowship F31CA200544 (E.C.W.).

### Author contributions

M.A.G., M.A.S., N.R.M., H.X., J.F.A.P., S.A.M., J.T.T., C.L.M., G.A. and P.A.W. all carried out experiments and interpreted data. M.A.G., H.X., E.C.W. and C.R.B. conceived the project. M.A.G., H.X., J.F.A.P., S.A.M., J.T.T., C.L.M., P.A.W., G.A. and E.C.W. synthesized, characterized and tested antibody conjugates. The tumor growth and leukocyte analyses were developed and carried out by M.A.S. (Figs. 4 and 5 and associated extended and

supplemental figures) and N.R.M. (Fig. 6 and associated supplemental and extended figures). S.A.M. was responsible for all peptide mass spectrometry. M.A.G., J.T.T. and particularly J.F.A.P. optimized the synthetic chemistry. M.A.G., H.X., J.F.A.P., G.A., P.A.W. and J.T.T. expressed and purified proteins and tested activities. M.A.G. and C.L.M. performed mouse imaging and lectin histology. M.A.G. and C.R.B. wrote the manuscript with input from all authors. H.L. and C.R.B. provided supervision.

### Competing interests

M.A.G., H.X., E.C.W. and C.R.B. are inventors of the patent filed by Stanford University (international publication number WO2018006034A1) titled 'Conjugates for targeted cell-surface editing' published on January 4, 2018 and licensed by Palleon Pharmaceuticals on 06/27/2017. C.R.B. is a cofounder and Scientific Advisory Board member of Palleon Pharmaceuticals, Enable Bioscience, Redwood Biosciences (a subsidiary of Catalent) and InterVenn Biosciences, and a member of the Board of Directors of Eli Lilly & Company. H.L. received research and traveling support from Bristol-Myers Squibb. H.L. received traveling support from Merck Sharp Dome and Roche. H.L. is a member of the Scientific Advisory Board of Palleon Pharmaceuticals.

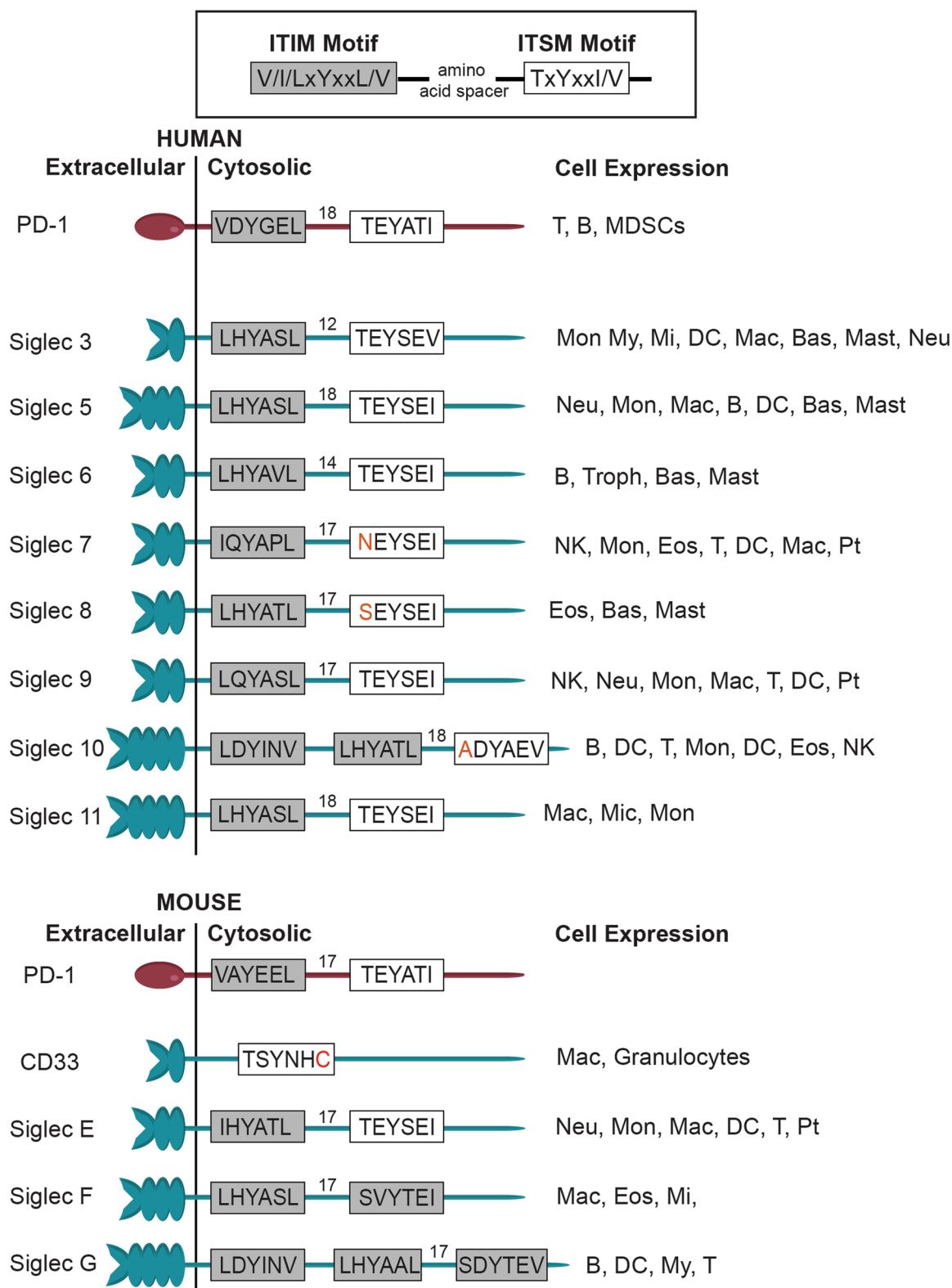
### Additional information

**Extended data** is available for this paper at <https://doi.org/10.1038/s41589-020-0622-x>.

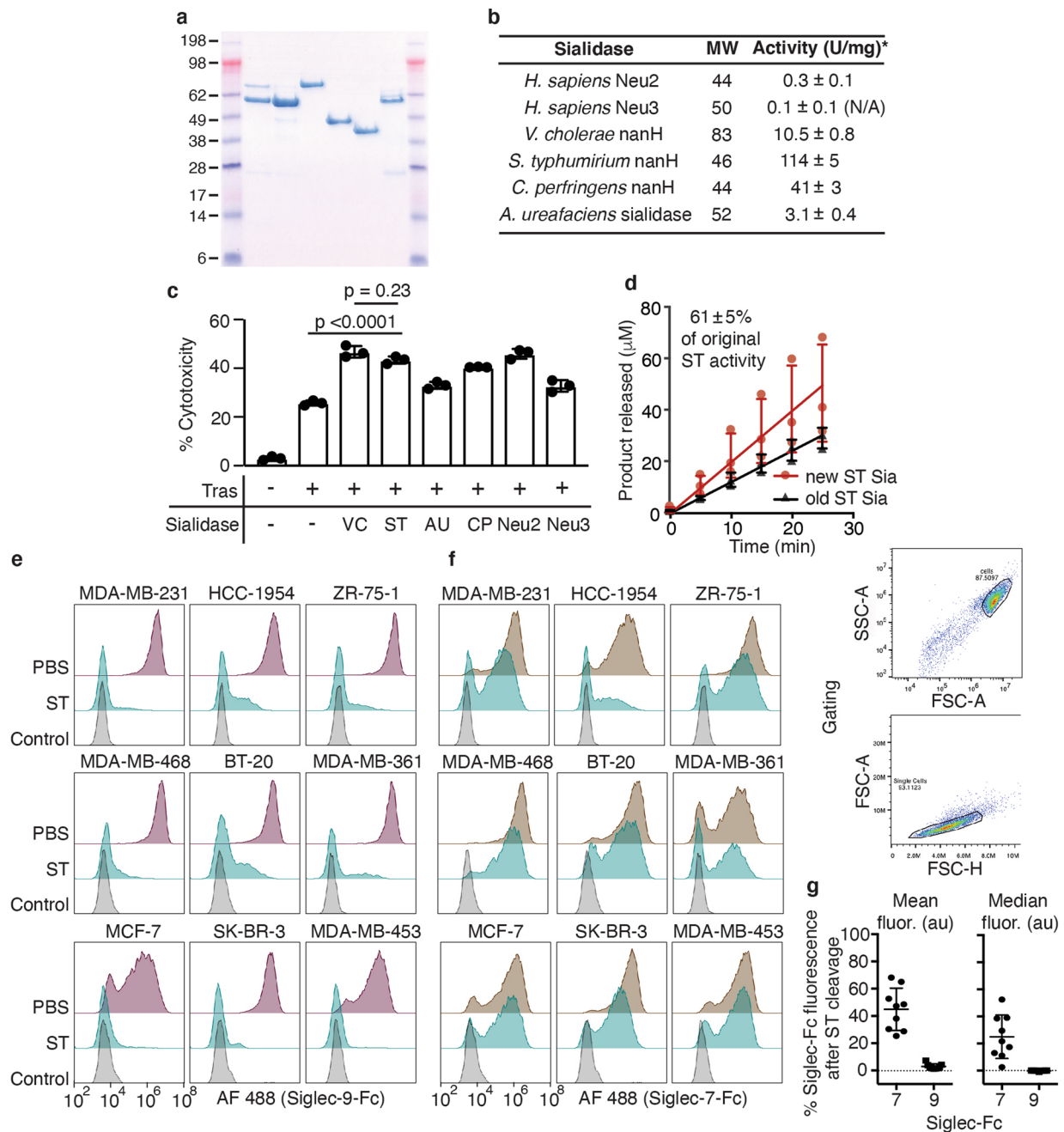
**Supplementary information** is available for this paper at <https://doi.org/10.1038/s41589-020-0622-x>.

**Correspondence and requests for materials** should be addressed to C.R.B.

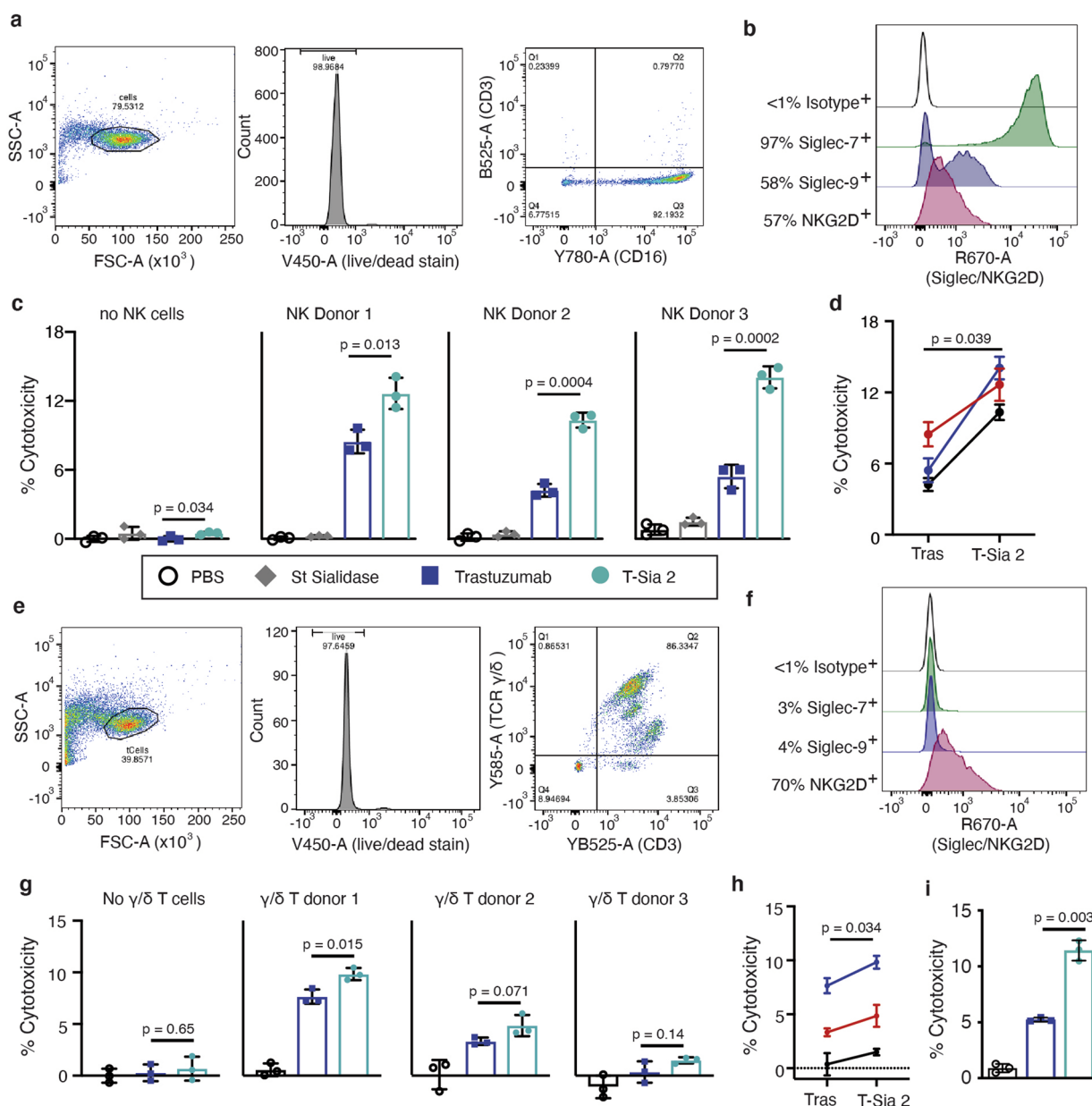
**Reprints and permissions information** is available at [www.nature.com/reprints](http://www.nature.com/reprints).



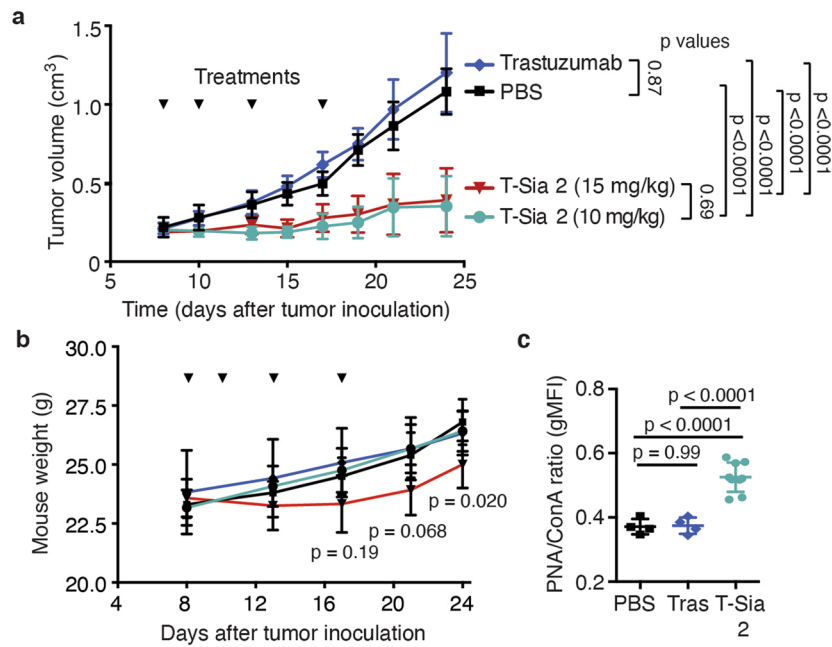
**Extended Data Fig. 1 | The PD-1 receptor and eight members of the human Siglec family have a homologous ITIM-ITSM cytosolic sequence motif and are expressed on a variety of immune cells.** Both PD-1 and Siglecs contain an N-terminal binding domain to their ligands (PD-L1/2 and sialoglycans, respectively), a helical single pass through the cell membrane, and an 82-126 amino acid cytosolic C-terminus containing an ITIM motif, a 12-18 amino acid spacer, and an ITSM or ITSM-like motif. Siglecs are expressed on a variety of immune cells; cell types that are Siglec<sup>+</sup> or have Siglec<sup>+</sup> subsets reported in humans and mice are indicated above for each Siglec receptor. T = T cell, B = B cell, MDSCs = myeloid-derived suppressor cells, My = Myeloid-precursor, Mon = Monocyte, Mi = Microglia, Neu = Neutrophil, Mac = Macrophage, Troph = Trophoblast, NK = Natural killer cell, Eos = Eosinophil, Bas = Basophil, DC = Dendritic cell, Mast = Mast cell, Pt = platelet. Siglec protein sequences are from Uniprot with added cell expression information from multiple sources<sup>10,14,15,46,54-60</sup>.



**Extended Data Fig. 2 | ST sialidase is a small, stable sialidase that enhances NK cell-mediated ADCC towards breast cancer cells and cleaves Siglec-7 and -9 ligands at high concentrations. a**, PAGE-SDS reducing gel of six recombinantly expressed and purified sialidases: Neu2, Neu3, *Vibrio cholerae* sialidase, *Salmonella typhimurium* NanH, *Clostridium perfringens* NanH, *Arthrobacter ureafaciens* NanH **b**, Molecular weights and specific activities (in  $\mu\text{mol}$  substrate converted per min per mg enzyme) of sialidases determined by *in vitro* activity assays with the fluorogenic substrate 4-MUNANA ( $n=3$  experimental replicates; mean  $\pm$  SD). **c**, IL2-activated NK cell-mediated ADCC assay against target BT-20 breast cancer cells treated with 10 nM trastuzumab (Tras) and  $2 \mu\text{M}$  sialidases at E/T = 4, percent cytotoxicity was detected by LDH release after 4 h. Figure shows mean  $\pm$  SD from  $n=3$  experimental replicates against the same biological NK cell donor. Statistical analysis by one way ANOVA with Tukey's multiple comparisons adjusted  $p$ -values. **d**, *In vitro* activity assay of freshly expressed sialidase compared with sialidase stored in PBS at  $4^\circ\text{C}$  for 2 years reveals that significant ST sialidase activity is preserved ( $n=3$  experimental replicates fit to a linear regression  $\pm$  SD). **e-g**, Siglec ligand depletion by ST sialidase cleavage is effective across many breast cancer cell lines. ST sialidase ( $2 \mu\text{M}$ ) was incubated with nine different breast cancer cell lines for 1 h and the removal of Siglec ligands compared to PBS-treated cells was assessed by staining with Siglec-9-Fc (**e**) or Siglec-7-Fc (**f**) and anti-human-488 secondary antibody (control: secondary only). Gating is shown on the right, first selecting the cell population (FSC-A/SSC), then gating on single cells (FSC-A/FSC-H). Representative images from  $n=2$  experimental replicates of the  $n=9$  biological cell line replicates each with  $>2,000$  cells are shown. The mean and median ( $\pm$  SD) percent decrease in Siglec ligand-binding fluorescent signal upon ST treatment of the  $n=9$  cell lines are quantified in **g**.

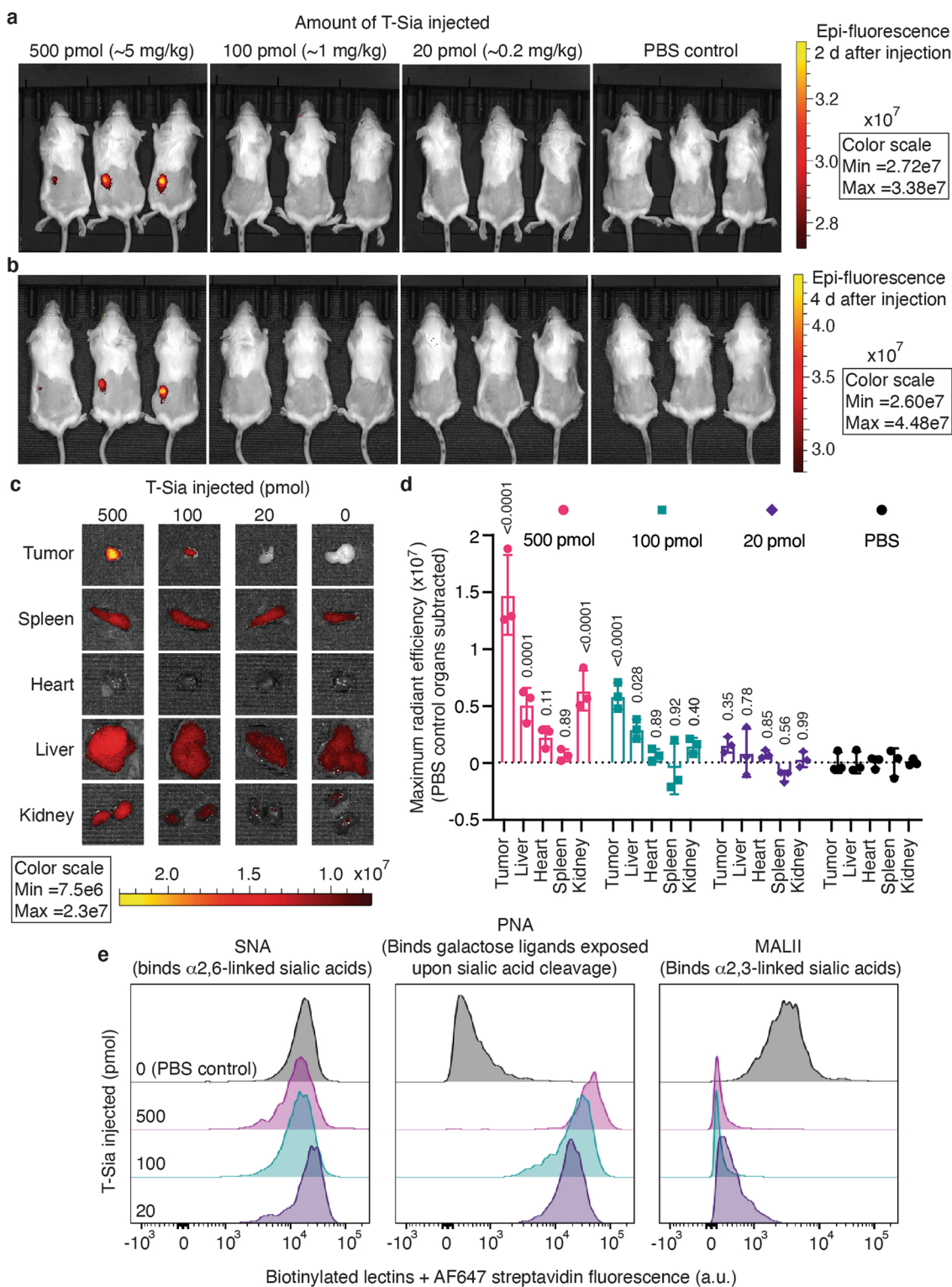


**Extended Data Fig. 3 | T-Sia 2 enhances NK cell-mediated and gamma-delta T cell-mediated ADCC *in vitro*.** **a**, Representative flow cytometry plots assessing purity of isolated primary NK cells. For n = 3 independent biological replicates of NK cell isolation, cells were >95% CD3<sup>-</sup> and had both CD16<sup>high</sup> and CD16<sup>low</sup> populations. **b**, NK cell-surface expression of some sialic acid-binding receptors from a representative NK donor. Isolated NK cells in all n = 3 biological replicates were positive for Siglec-7, had mixed expression of Siglec-9, and had low-to-moderate unimodal expression of NKG2D. **c**, NK cell-mediated ADCC of BT-20 target cells treated with PBS, 20 nM free ST sialidase, 10 nM trastuzumab, or 10 nM T-Sia 2 (mean ± SD). Plots from BT-20 cells alone (left) and from incubation with NK cells are each from n = 3 experimental replicates, E/T = 4, no IL-2 activation, detecting LDH release after 4 h; statistical analysis by two-tailed t tests. **d**, Plotting the NK cell-mediated cytotoxicity of trastuzumab and T-Sia 2-treated cells from (c) shows that desialylation enhances ADCC significantly across the n = 3 biological NK cell donor replicates. Mean ± SD, analyzed by a paired two-tailed t test. **e**, Representative gating showing the purity of isolated primary  $\gamma\delta$  T cells. Consistent with n = 3 biological replicates,  $\gamma\delta$  T Cells are somewhat impure (only ~85% are  $\gamma\delta$ <sup>+</sup> and CD3<sup>+</sup>) and there are apparent sub-populations. **f**, A representative histogram (from n = 3 biological replicates) of a typical donor demonstrates that these cells are negative for Siglec-7 and -9 expression, although they also have a moderate unimodal expression of NKG2D. **g**, Mean ± SD from  $\gamma\delta$  T cell-mediated ADCC assays targeting HER2<sup>+</sup> EMT6 cells treated with PBS, 20 nM free ST sialidase, 10 nM trastuzumab, or 10 nM T-Sia 2. Results are shown from n = 3 independent experimental replicates on EMT6 cells alone (left) and from incubation with IL-2 activated  $\gamma\delta$  T cells isolated from n = 3 distinct biological donors, E/T = 1, detecting LDH release after 8 h; statistical analysis by two-tailed t tests. **h**, Comparing trastuzumab vs T-Sia 2 treatment across n = 3 biological NK donors from (g), shows significant enhancement of cytotoxicity by desialylation. Mean ± SD, statistical analysis by a paired two-tailed t test. **i**, An IL-2 activated  $\gamma\delta$  T cell-mediated ADCC assay targeting SK-BR-3 cells incubated with PBS, trastuzumab (10 nM) or T-Sia 2 (10 nM), (n = 3), E/T = 3, detecting LDH release after 6 h; (Mean ± SD), statistical analysis by two-tailed t test.



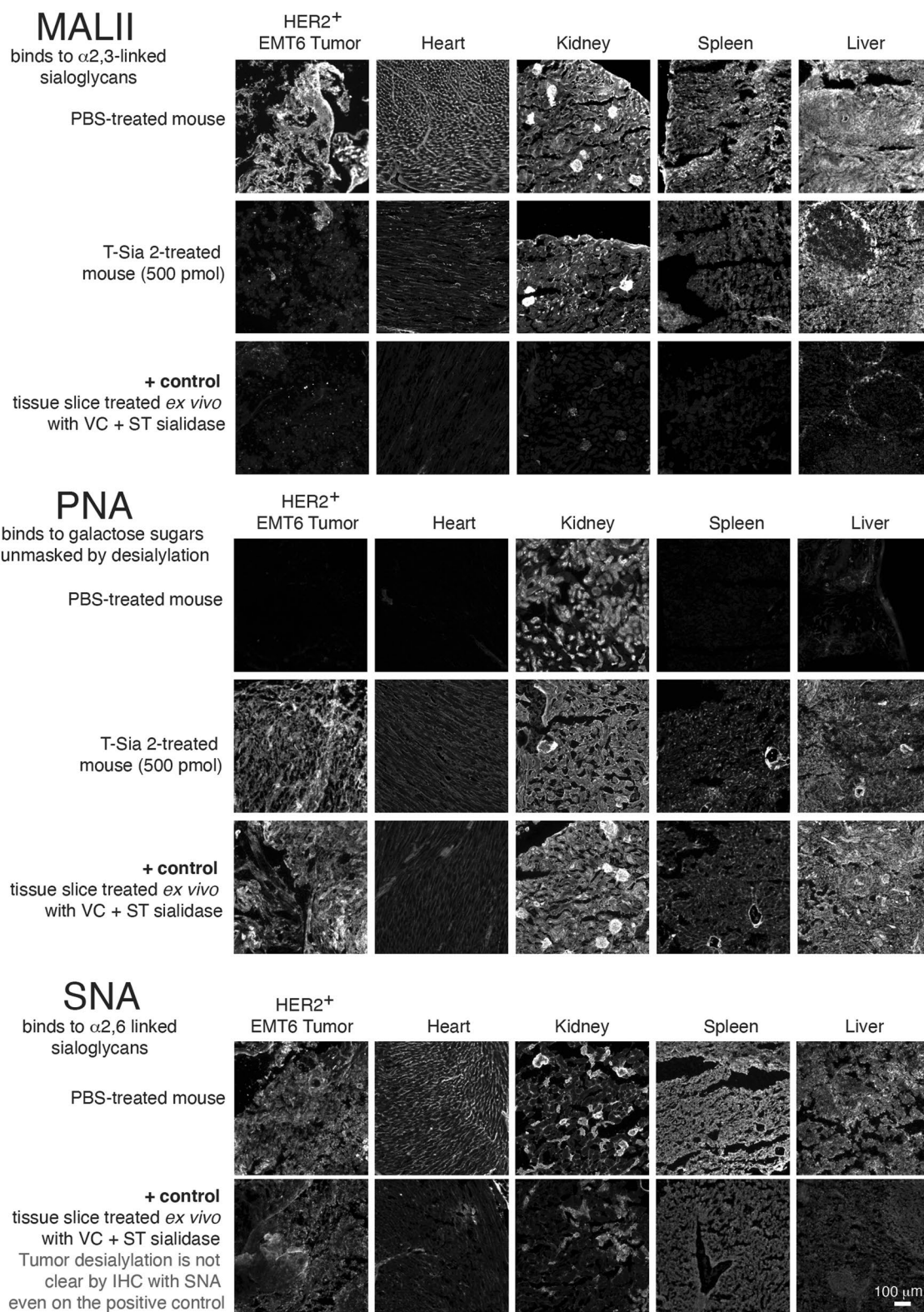
**Extended Data Fig. 4 | T-Sia 2 treatment desialylates EMT6 tumors and delays tumor growth compared to trastuzumab- or PBS-treatment.**

**a**, Mean  $\pm$  SD tumor volume over time for HER2<sup>+</sup> EMT6 tumor-bearing mice described in Fig. 4b, treated with PBS (n = 5), trastuzumab (10 mg/kg injection, n = 6), T-Sia 2 (10 mg/kg injection, n = 6), and T-Sia 2 (15 mg/kg injection, n = 6). RM two-way ANOVA with adjusted p-values from Tukey's multiple comparisons between groups shown. **b**, Mouse weight from all of the mice in (a) measured 5x over the course of 24 days of treatment and tumor growth. Ordinary two-way ANOVA with Dunnett's multiple comparisons to PBS mice, multiplicity-adjusted p-values for T-Sia (15 mg/kg) compared to PBS are shown at three time points, (mean  $\pm$  SD). **c**, Lectin flow cytometry staining with fluorescent PNA to detect exposed galactose of extracted tumor cells from mice in Fig. 4b upon their sacrifice 13–23 days after final administration of PBS, trastuzumab, or T-Sia 2, (geometric mean (gMFI)  $\pm$  SD), normalized to ConA fluorescence (a control that binds to mannose on cells), n = 4 (trastuzumab, PBS) n = 9 (T-Sia 2). Ordinary one-way ANOVA with adjusted p-values shown from Tukey's multiple comparisons.



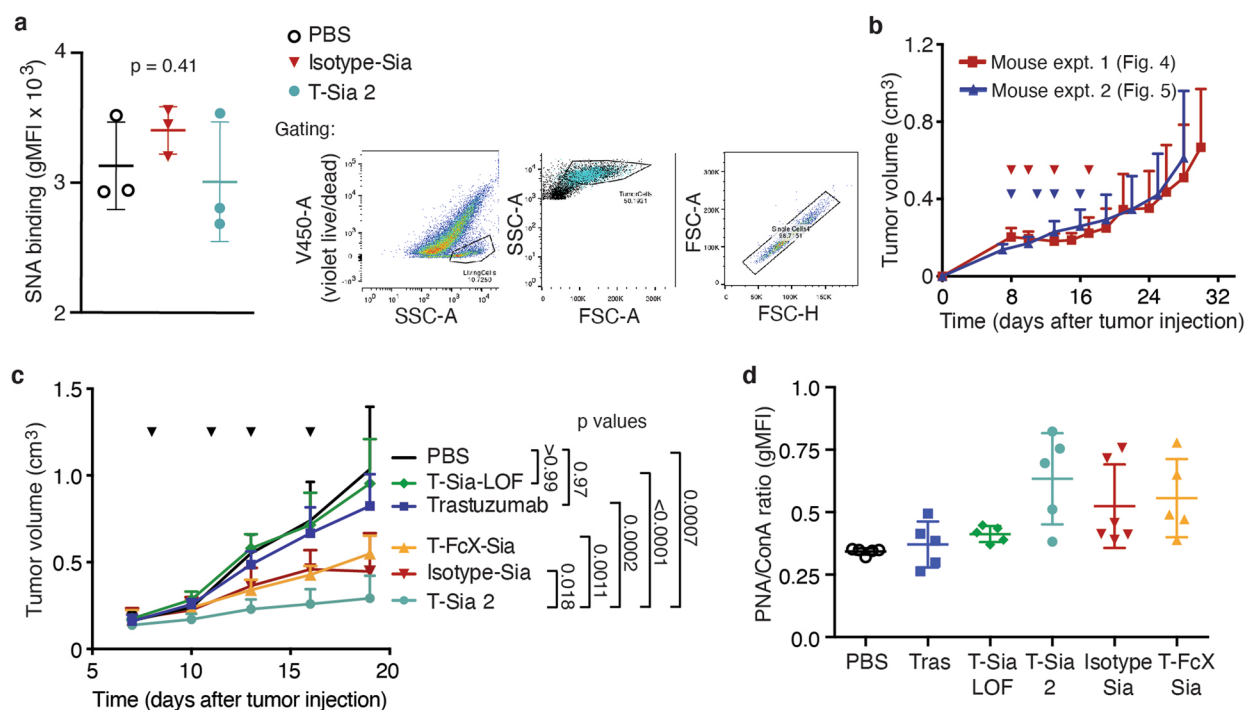
Extended Data Fig. 5 | See next page for caption.

**Extended Data Fig. 5 | T-Sia 2 accumulates in the HER2<sup>+</sup> EMT6 tumors in mice and can desialylate tumor cells at a single injection concentration as low as 0.2 mg/kg.** Mice bearing HER2<sup>+</sup> EMT6 subcutaneous tumors on their left flanks were imaged using non-invasive *in vivo* fluorescence imaging at **a**, 48 h, and **b**, 4 days after IR800-labeled T-Sia 2 was injected IP into n = 3 mice per dose: 500 pmol, 100 pmol, 20 pmol, and PBS control. All mice are shown above. **c**, Representative photographs overlaid with fluorescent images of the tumor, spleen, heart, liver, and kidneys removed 4 days after conjugate injection, showing where fluorescently-labeled T-Sia 2 was localized. These images are representative of n = 3 biological mouse replicates. **d**, Maximum radiant efficiency was quantified for the n = 3 replicate mice per group and normalized to the average of the PBS mouse organ control. Mean  $\pm$  SD are displayed with p values from a two-way ANOVA with Dunnett's multiple comparisons to the respective control organ of mice injected with PBS. **e**, N = 3 tumors taken from each mouse group were pooled, resuspended, and single tumor cells were analyzed for lectin staining by flow cytometry. Although the SNA ligands *in vivo* were insensitive to T-Sia 2 desialylation at these doses, dramatic desialylation was apparent by detecting with the more sensitive reagents PNA (detecting exposed galactosyl ( $\beta$ -1,3) N-acetylgalactosamine) and MALII (detecting  $\alpha$ 2,3 linked sialic acids). The x-axis is displayed on a biexponential scale, y-axis is cell count normalized to mode. For MALII, SNA, and PNA staining n > 2,600 cells for all histograms except the 500 pmol T-Sia 2-dosed-mice histograms only represent n = 827 and n = 1,809, and n = 234 cells, respectively, as the treated tumors were very small. These tumor desialylation results are from one independent mouse experiment with n = 3 biological replicates (mouse tumors); and are consistent with other experiments in this work showing mouse tumor desialylation with SNA, PNA, and MAL II (Fig. 5c, and Extended Data Figs. 4c, 6, and 7a). Color bars are in units of radiant efficiency.

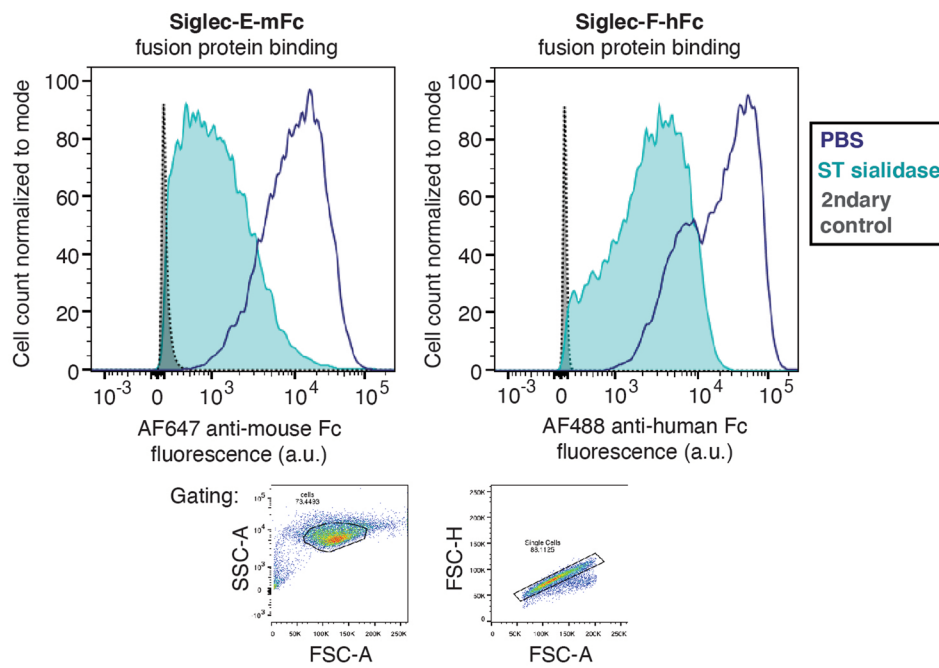


Extended Data Fig. 6 | See next page for caption.

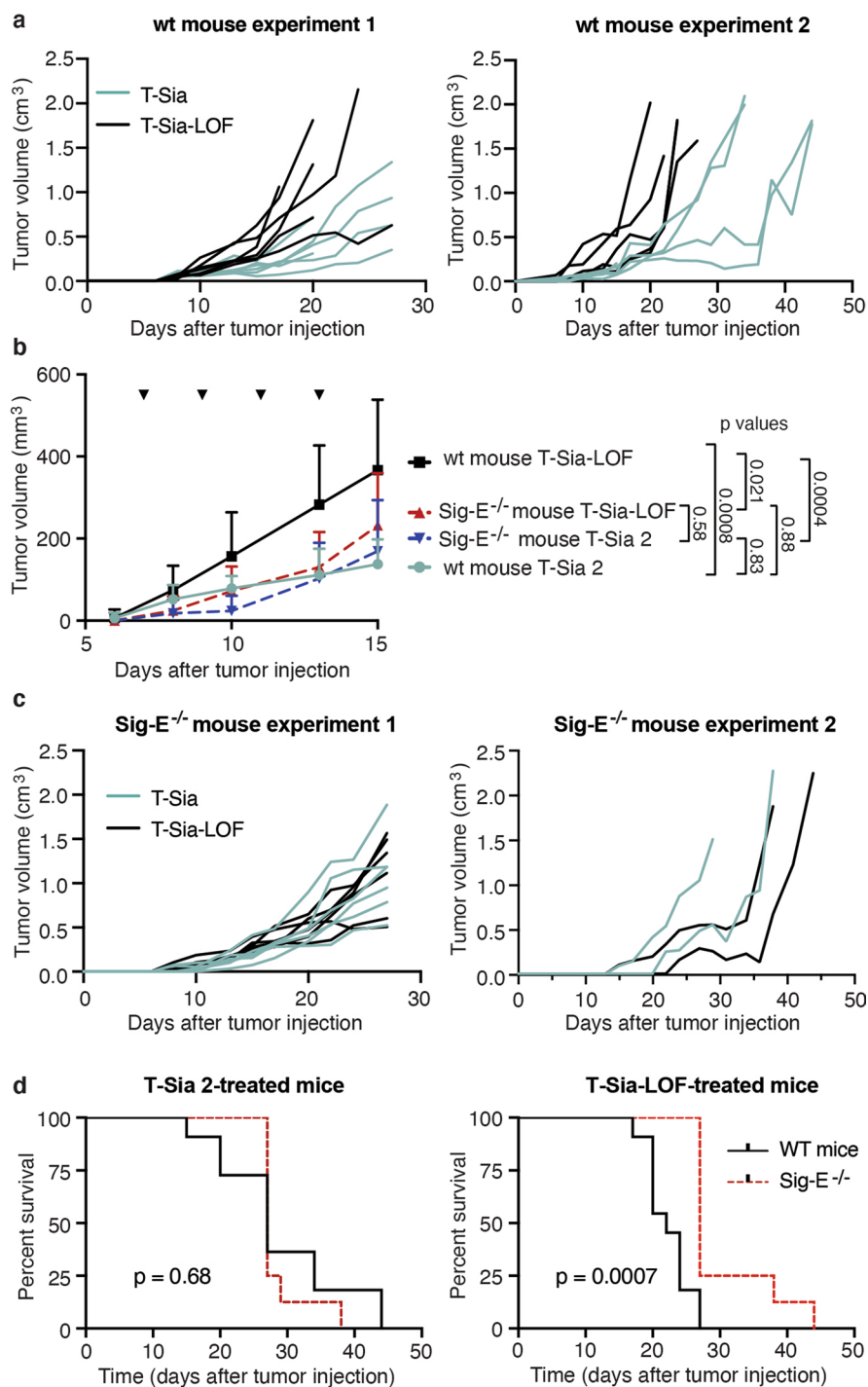
**Extended Data Fig. 6 | Representative lectin immunohistochemistry of tumor and organ slices show desialylation that can be detected in all examined organs.** Sialoglycan degradation is detectable by fluorescence microscopy of stained tumor and organ slices from the mice in Extended Data Fig. 5 treated with 500 pmol T-Sia 2. Staining with Maackia Amurensis Lectin II (MALII, top images), which preferentially binds sialic acid in an ( $\alpha$ -2,3) linkage, reveals a dramatic decrease in fluorescent signal from binding ( $\alpha$ -2,3) sialic acid in the tumor, comparable to positive control tissue slices treated with a sialidase cocktail *ex vivo*. In the heart, kidney, and spleen, a moderate decrease in fluorescence can also be perceived. Staining with Peanut Agglutinin (PNA, middle images), which binds preferentially to exposed galactose upon desialylation, is increased in the tumor tissue upon desialylation, this effect is also quite apparent in the heart, spleen, and liver, kidney. Staining with *Sambucus nigra* (Elderberry Bark) lectin (SNA), which preferentially binds sialic acid in an ( $\alpha$ -2,6) linkage, was not performed on the T-Sia 2 samples as there was consistently little to no difference between tumor staining in the PBS control mice and in tumor slices treated *ex vivo* with a high concentration of ST and VC sialidase, indicating that SNA signal in the tumor tissue in the mouse is either background or represents signal from glycans that are not readily cleavable by ST or VC sialidase, this finding is in agreement with tumor lectin staining by flow cytometry (Extended Data Figs. 5 and 7). All images are representative of at least  $n = 3$  organ images per mouse taken from  $n = 3$  different mice injected with 500 pmol T-Sia 2.



**Extended Data Fig. 7 | Testing the control sialidase-conjugates against the HER2<sup>+</sup> EMT6 tumor model.** For flow cytometry analysis of sialoglycan degradation, a single 20 pmol injection of T-Sia 2, Isotype-Sia, or PBS control was injected IP into mice with subcutaneous HER2<sup>+</sup> EMT6 cells. After four days, tumors were harvested. **a**, Staining with *Sambucus nigra* (Elderberry Bark) lectin (SNA), which preferentially binds sialic acid in an ( $\alpha$ -2,6) linkage, did not show significant desialylation changes between these samples,  $n = 3$  mice, geometric mean  $\pm$  SD. Right: gating strategy: dead cells and tumor debris were gated out (V450-A/SSC-A), followed by gating on size (FSC-A/SSC-A - \*blue cells depict where HER2<sup>+</sup> stained cells fall in the gate). Finally, single cells are gated with FSC-A/FSC-H. **b**, Growth curves of the HER2<sup>+</sup> EMT6 tumors of mice treated with T-Sia 2 (10 mg/kg) were consistent between the first tumor growth mouse experiment (shown in red, depicted in Fig. 4c,  $n = 6$  mice) and the second independent experiment (blue, depicted in Fig. 5d,  $n = 7$  mice); data are reported as mean  $\pm$  SD. **c**, Average (mean  $\pm$  SD) tumor growth of all the mice in Fig. 5d plotted together until the first mouse death (day 19). Mice were injected IP with PBS ( $n = 6$ ), 10 mg/kg trastuzumab (tras) ( $n = 6$ ), T-Sia-LOF ( $n = 6$ ), Isotype-Sia ( $n = 6$ ), T-FcX-Sia ( $n = 7$ ), or T-Sia 2 ( $n = 7$ ). A two-way ANOVA was performed with adjusted  $p$ -values from Tukey's multiple comparisons. **d**, Lectin stain with PNA of exposed galactose from extracted tumor cells taken from the mice in Fig. 5d, e after mouse sacrifice. Geometric mean  $\pm$  SD of PNA/ConA, ( $n = 5$ : PBS, Tras, T-Sia-LOF, T-FcX-Sia;  $n = 6$ : Isotype-Sia).

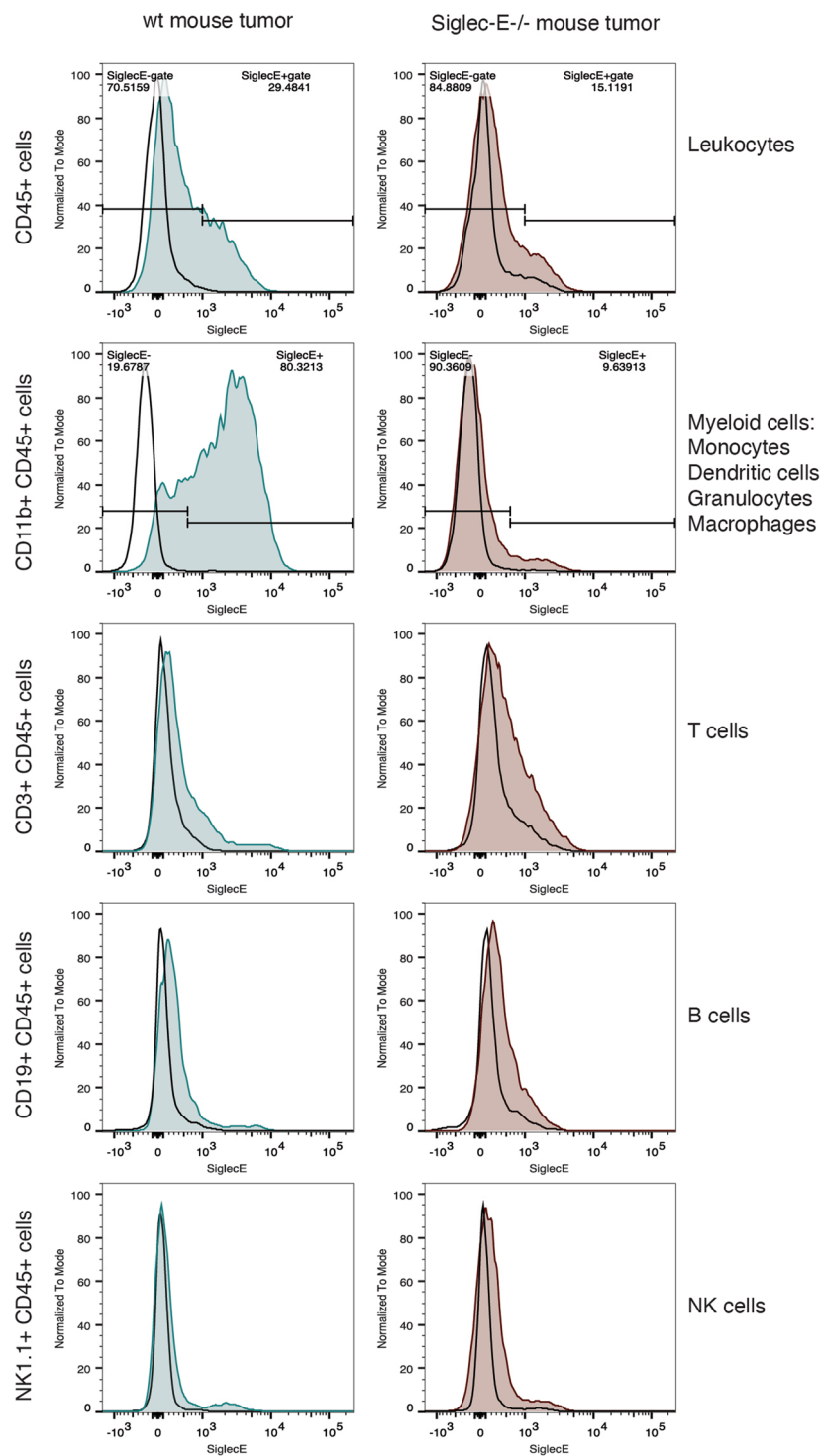


**Extended Data Fig. 8 | ST sialidase can cleave Siglec ligands from HER2<sup>+</sup> B16D5 cells.** HER2<sup>+</sup> B16D5 cells cultured *in vitro* bound to commercially available mouse Siglec-Fc proteins (Siglecs -E and -F-Fc). The Siglec ligands detected on the B16D5 cells were sensitive to 2  $\mu$ M ST sialidase treatment for 1 h. y-axis shows cell count normalized to mode, x-axis is on a bi-exponential scale, >13,500 cells per histogram. PBS control-treated cells are shown in outlined dark blue with, ST sialidase-treated cells are colored teal, secondary only control stains are shown in gray. Gating is shown below, cells were selected by SSC-A/FSC-A gating, followed by selection of single cells by linear gating on FSC-A vs FSC-H. Data are representative of n=3 independently performed experiments on HER2<sup>+</sup> B16D5 cells.



**Extended Data Fig. 9 | HER2<sup>+</sup> B16D5 tumor growth curves of wt and Sig-E<sup>-/-</sup> C57BL/6 mice treated with T-Sia 2 or the loss of function T-Sia-LOF.**

**a**, Tumor growth curves of (left): wt mouse experiment 1 with  $n=6$  mice per group, and (right): wt mouse experiment 2 with  $n=5$  mice per group. **b**, Average tumor growth of wt and Sig-E<sup>-/-</sup> mice treated with either T-Sia 2 or T-Sia-LOF inactive control. Data shown are mean  $\pm$  SD until the date of the first mouse death (day 15), analyzed by RM two way ANOVA with from Tukey's multiple comparisons test. Sample sizes are  $n=11$  for wt mice (T-Sia 2 and T-Sia-LOF) and  $n=8$  for Sig-E<sup>-/-</sup> mice (T-Sia 2 and T-Sia-LOF). **c**, Individual tumor growth curves with Siglec-E deficient mice (left): mouse experiment 1 ( $n=6$  mice per group), and (right): experiment 2 ( $n=2$  mice per group). **d**, Survival curves based on euthanasia criteria with HER2<sup>+</sup> B16D5 tumors from Fig. 6a,b demonstrate that knocking out Siglec-E in this mouse tumor model benefits mouse survival. For T-Sia LOF-treated mice, the Sig-E<sup>-/-</sup> mice have prolonged survival compared to wt mice. For T-Sia 2-treated mice, sialoglycan degradation of the wt mice extends the survival to an outcome similar to the Sig-E<sup>-/-</sup> mice. P-values are shown from a log-rank (Mantel-Cox) test,  $n=11$  wt mice treated with T-Sia 2 or T-Sia-LOF,  $n=8$  for Sig-E<sup>-/-</sup> treated with T-Sia 2 or T-Sia-LOF.



**Extended Data Fig. 10 | B16D5 tumors in C57Bl/6 mice have significant infiltration of Siglec-E<sup>+</sup> immune cells, which can largely be attributed to Siglec-E expressing CD11b<sup>+</sup> leukocytes.** Representative histograms of tumor infiltrating leukocytes gated as shown in Supplementary Fig. 22, with Siglec-E expression on the biexponential x-axis and cell count normalized to mode ( $n=10$  for wt mice,  $n=12$  for Siglec-E deficient mice). A fluorescence minus one control (FMO, negative control that lacks the Siglec-E antibody) for each sample is shown as a black outline. Total leukocytes (defined as CD45<sup>+</sup> cells) show a detectable increased Siglec-E expression in wild-type mice (blue) compared to Siglec-E<sup>-/-</sup> mouse controls (red). Investigating further, T cells, B cells, and NK cells (represented by CD3<sup>+</sup>, CD19<sup>+</sup>, and NK1.1<sup>+</sup> leukocyte populations) did not show significant Siglec-E expression compared to Sig-E<sup>-/-</sup> control cells, however, myeloid (CD11b<sup>+</sup>) cells, which include macrophages, granulocytes, certain dendritic cells, and monocytes, had significant anti Siglec-E signal and represent the vast majority of Siglec-E<sup>+</sup> leukocytes in these tumors.

## Reporting Summary

Nature Research wishes to improve the reproducibility of the work that we publish. This form provides structure for consistency and transparency in reporting. For further information on Nature Research policies, see [Authors & Referees](#) and the [Editorial Policy Checklist](#).

### Statistics

For all statistical analyses, confirm that the following items are present in the figure legend, table legend, main text, or Methods section.

n/a Confirmed

- The exact sample size ( $n$ ) for each experimental group/condition, given as a discrete number and unit of measurement
- A statement on whether measurements were taken from distinct samples or whether the same sample was measured repeatedly
- The statistical test(s) used AND whether they are one- or two-sided  
*Only common tests should be described solely by name; describe more complex techniques in the Methods section.*
- A description of all covariates tested
- A description of any assumptions or corrections, such as tests of normality and adjustment for multiple comparisons
- A full description of the statistical parameters including central tendency (e.g. means) or other basic estimates (e.g. regression coefficient) AND variation (e.g. standard deviation) or associated estimates of uncertainty (e.g. confidence intervals)
- For null hypothesis testing, the test statistic (e.g.  $F$ ,  $t$ ,  $r$ ) with confidence intervals, effect sizes, degrees of freedom and  $P$  value noted  
*Give  $P$  values as exact values whenever suitable.*
- For Bayesian analysis, information on the choice of priors and Markov chain Monte Carlo settings
- For hierarchical and complex designs, identification of the appropriate level for tests and full reporting of outcomes
- Estimates of effect sizes (e.g. Cohen's  $d$ , Pearson's  $r$ ), indicating how they were calculated

*Our web collection on [statistics for biologists](#) contains articles on many of the points above.*

### Software and code

Policy information about [availability of computer code](#)

#### Data collection

A BD Accuri C6 Plus flow cytometer, LSRII, and a Fortessa LSR II flow cytometer were used for flow cytometry data acquisition. Image Studio Software (v 5.2) was used for gel scanning. A SpectraMax i3x plate reader was used for absorbance and fluorescence detection in a 96 well plates. The NanoDrop 2000 Spectrophotometer (Thermo Fisher) was used to characterize proteins. An IncuCyte S3 Live Cell Analysis system (Sartorius) equipped with a 10x objective lens in phase contrast and red fluorescence (ex: 585 +/- 20, em: 665 +/- 40, acquisition time, 800 ms) was used to monitor live cell fluorescence over time. An Orbitrap Fusion Tribrid mass spectrometer was used to analyze protein tryptic digest masses and a Bruker MicroTOF-Q II time-of-flight mass spectrometer was used for full-length protein analysis. The Octet Red 96 was used for biolayer interferometry. A 1100/1200 series instrument (Agilent Technologies) was used for HPLC analysis. Fluorescence images of tissues were acquired using an Axio Observer Z-1 (Zeiss) equipped with a Spectra-X Light engine LED light (Lumencor), controlled with Micro-Manager. Complete blood counts were measured on the ADVIA120 Hematology Analyzer using the Multispecies Version 5.9.0-MS software (Bayer)

#### Data analysis

MestReNova (v 12.0.3) was used for all chemical NMR analysis. Microsoft Excel (v14.5.1) and GraphPad Prism (v6) were used for data analysis and curve-fitting. FlowJo (v10.0) was used for flow cytometry data analysis. For mass spectrometry, all cysteine-containing peptides were manually sequenced using Xcalibur software.

For manuscripts utilizing custom algorithms or software that are central to the research but not yet described in published literature, software must be made available to editors/reviewers. We strongly encourage code deposition in a community repository (e.g. GitHub). See the Nature Research [guidelines for submitting code & software](#) for further information.

## Data

Policy information about [availability of data](#)

All manuscripts must include a [data availability statement](#). This statement should provide the following information, where applicable:

- Accession codes, unique identifiers, or web links for publicly available datasets
- A list of figures that have associated raw data
- A description of any restrictions on data availability

All data shown in this manuscript are provided either as source data files or in Supplementary Dataset 1 (.xlsx). Any unique materials presented in the manuscript may be available from the authors upon reasonable request and through a materials transfer agreement.

## Field-specific reporting

Please select the one below that is the best fit for your research. If you are not sure, read the appropriate sections before making your selection.

- Life sciences       Behavioural & social sciences       Ecological, evolutionary & environmental sciences

For a reference copy of the document with all sections, see [nature.com/documents/nr-reporting-summary-flat.pdf](https://nature.com/documents/nr-reporting-summary-flat.pdf)

## Life sciences study design

All studies must disclose on these points even when the disclosure is negative.

Sample size	No sample size calculation was performed. Typically three experimental replicates were performed in order to show standard deviations for in vitro experiments. Exceptions: Supplementary Fig. 5a, MDA-MB-361, E/T=8, PBS sample there is only n=2 as noted in the figure legend, there were not enough cells during one of the experimental replicates. Additionally Supplementary Fig. 8c has only n=2 experimental replicates, and the biolayer interferometry was only repeated n=2 times - none of these data are essential to the main results of the paper. For the mouse studies, 5-7 mice per group were used, this was recommended by our co-authors as group sizes that would be likely to provide significant data while not being wasteful of the lives of laboratory animals. The exception to this is the second experimental replicate of the Siglec-E KO mouse experiment, where Siglec-E mice were limited to n=2 per group.
Data exclusions	There were no data exclusions. In certain cases, only a subset of the mouse tumors were analyzed for TILs or lectin staining due to ulceration, but all those analyzed were reported.
Replication	All data were confirmed with multiple replicates as noted in the methods and figure legends. In vitro NK killing assay values were very consistent when experiments were replicated with a single NK cell donor, but % cytotoxicity values shifted significantly depending on the primary NK cell donor used. We show NK cell ADCC assays with multiple NK donors in Supplementary Fig. 5, Extended Data Fig. 3, and in Fig 4a to show that the trend for increased % cytotoxicity when treated with T-Sia 2 is consistent across multiple donors. Protein-conjugates were only characterized by n=1 intact-protein mass spectrum as is typical, protein conjugation reactions were repeated at least n=2 times with a small scale and a larger scale reaction, each time the correct intact-protein mass was confirmed for the reaction by MS.
Randomization	No randomization.
Blinding	No blinding was performed for in vitro assays. The scientist performing the in vivo EMT6 tumor growth studies was blinded for the injections and tumor measurements, the scientists who performed the in vivo glycosylation and targeting analysis as well as the Siglec-E KO growth experiments in Fig. 6 were not blinded.

## Reporting for specific materials, systems and methods

We require information from authors about some types of materials, experimental systems and methods used in many studies. Here, indicate whether each material, system or method listed is relevant to your study. If you are not sure if a list item applies to your research, read the appropriate section before selecting a response.

### Materials & experimental systems

n/a	Included in the study
<input type="checkbox"/>	<input checked="" type="checkbox"/> Antibodies
<input type="checkbox"/>	<input checked="" type="checkbox"/> Eukaryotic cell lines
<input checked="" type="checkbox"/>	<input type="checkbox"/> Palaeontology
<input type="checkbox"/>	<input checked="" type="checkbox"/> Animals and other organisms
<input checked="" type="checkbox"/>	<input type="checkbox"/> Human research participants
<input checked="" type="checkbox"/>	<input type="checkbox"/> Clinical data

### Methods

n/a	Included in the study
<input checked="" type="checkbox"/>	<input type="checkbox"/> ChIP-seq
<input type="checkbox"/>	<input checked="" type="checkbox"/> Flow cytometry
<input checked="" type="checkbox"/>	<input type="checkbox"/> MRI-based neuroimaging

Antibodies used	<p>Alexa Fluor® 647 anti-human Her2 antibody Biolegend (324412) FC, 1:100  FITC Conjugated Sambucus nigra (Elderberry Bark) -SNA-I-, 1mg EY Laboratories (F-6802-1) FC, 1:100  Siglec-7-Fc Chimera protein R&amp;D Systems (1138-SL-050) FC, 1:50  Siglec-9-Fc Chimera protein R&amp;D Systems (1139-SL-050) FC, 1:50  Siglec-F-Fc Chimera protein R&amp;D Systems (1706-SF-050) FC, 1:50  Alexa Fluor® 488 AffiniPure Goat Anti-Human IgG, Fcy fragment specific Jackson ImmunoResearch (109-545-008) FC, 1:375  PE/Dazzle™ 594 anti-mouse CD3 Antibody Biolegend (100246) FC, 1:100  Brilliant Violet 605™ anti-mouse CD4 antibody Biolegend (100548) FC, 1:100  Brilliant Violet 785™ anti-mouse CD8a Antibody Biolegend (100750) FC, 1:100  Alexa Fluor® 488 Rat Anti-CD11b BD Pharmingen (557672) FC, 1:100  PE-Cy™7 Hamster Anti-Mouse CD11c BD Biosciences (561022) FC, 1:100  BV421 Rat Anti-Mouse CD19 BD Pharmingen (562701) FC, 1:100  FITC anti-mouse CD25 Antibody Biolegend (102005) FC, 1:100  CD45 Monoclonal Antibody (30-F11), PerCP-Cyanine5.5 eBioscience (45-0451-82) FC, 1:100  APC anti-mouse CD69 Antibody Biolegend (104514) FC, 1:100  APC anti-mouse CD206 (MMR) Antibody Biolegend (141708) FC, 1:50  PE Rat Anti-Mouse CD335 (Nkp46) Clone 29A1.4 BD (560757) FC, 1:50  Alexa Fluor® 647 anti-mouse/rat/human FOXP3 Antibody Biolegend (320014) FC, 1:100  APC/Cyanine7 anti-mouse I-A/I-E Antibody Biolegend (107628) FC, 1:200  Brilliant Violet 421™ anti-mouse F4/80 Antibody Biolegend (123132) FC, 1:100  FITC Mouse anti-Human Granzyme B Clone GB11 BD (560211) FC, 1:100  PE/Cy7 Streptavidin Biolegend (405206) FC, 1:400  Biotinylated Concanavalin A (Con A) Vector Labs (B-1005) FC, 10 µg/mL  Biotinylated Peanut Agglutinin (PNA) Vector Labs (B-1075) FC, 10 µg/mL, IHC: 20 µg/mL  Biotinylated Maackia Amurensis Lectin II (MALII) Vector Labs (B-1265) FC, 10 µg/mL, IHC: 20 µg/mL  Biotinylated Sambucus Nigra Lectin (SNA, EBL) Vector Labs (B-1305) FC, 10 µg/mL, IHC: 20 µg/mL  Streptavidin Streptavidin, Alexa Fluor™ 647 conjugate Thermo (S21374) FC: 2 µg/mL, IHC: 15 µg/mL  APC anti-human CD328 (Siglec-7) BioLegend (339206) FC, 1:10  APC Mouse IgG1, κ Isotype Ctrl BioLegend (400122) FC, 1:10  APC anti-human Siglec-9 BioLegend (351506) FC, 1:10  FITC anti-human CD3 BioLegend (300306) FC, 1:10  PE anti-human TCR γ/δ BioLegend (331210) FC, 1:10  PE/Cy7 anti-human CD16 BioLegend (302016) FC, 1:10  CD314 (NKG2D) Monoclonal Antibody APC eBioscience™ (14-5879-82) FC, 1:10  APC/Cyanine7 anti-mouse CD19 Antibody Biolegend (115529) FC, 1:200  PE anti-mouse CD3ε Antibody Biolegend (100308) FC, 1:200  NK1.1 Monoclonal Antibody (PK136) PE- Cyanine7, eBioscience (25-5941-82) FC, 1:200  PE anti-Siglec-E Antibody, Biolegend (677104) FC, 1:50  FITC anti-mouse/human CD11b Antibody, Biolegend (101206) FC, 1:300  BV786 Rat Anti-Mouse CD4, BD Horizon (563331) FC, 1:100  Brilliant Violet 605 anti-mouse CD8a Antibody, Biolegend (100744), FC, 1:100  Zombie UV Fixable Viability Kit Biolegend (423108) FC, 1:200</p>
Validation	No further validation of antibodies was performed

## Eukaryotic cell lines

Policy information about [cell lines](#)

Cell line source(s)	MDA-MB-361, MDA-MB-231, MDA-MB-453, BT-20, ZR-75-1, MCF7, HCC1954, K562, HEK293, and BT474 were obtained from the American Tissue Culture Collection (ATCC). EMT6 cells expressing the HER2 protein were obtained from the Zippelius lab. The HEK-Blue cell line was obtained from Invivogen. B16D5 cells expressing the HER2 protein were a gift from the Weiner lab
Authentication	Cell lines have not been subjected to additional authentication.
Mycoplasma contamination	All cell lines regularly tested negative for mycoplasma infection by the Lonza MycoAlert Mycoplasma Detection Assay
Commonly misidentified lines (See <a href="#">ICLAC</a> register)	No commonly misidentified cells were used in this study

## Animals and other organisms

Policy information about [studies involving animals](#); [ARRIVE guidelines](#) recommended for reporting animal research

Laboratory animals	7-9 week old female Balb/c mice were used in the EMT6 tumor model, imaging study, and histology 10-12 week old male and female mice were used in the C57Bl/6 experiments with wt and Siglec-E knockout mice
--------------------	--

Wild animals	No wild animals were involved in this study
Field-collected samples	The study did not involve field-collected samples
Ethics oversight	Mouse tumor growth experiments were approved by the local Ethical Committee (Basel Stadt) Mouse imaging experiments were performed at Stanford University, mouse care was monitored by the Veterinary service center at Stanford University under APLAC protocol number 31511.

Note that full information on the approval of the study protocol must also be provided in the manuscript.

## Flow Cytometry

### Plots

Confirm that:

- The axis labels state the marker and fluorochrome used (e.g. CD4-FITC).
- The axis scales are clearly visible. Include numbers along axes only for bottom left plot of group (a 'group' is an analysis of identical markers).
- All plots are contour plots with outliers or pseudocolor plots.
- A numerical value for number of cells or percentage (with statistics) is provided.

### Methodology

Sample preparation	Sample preparations are described in the methods
Instrument	BD-Accuri C6 Plus and Fortessa LSR II, as well as the LSR II (BD)
Software	data analysis was performed using the FlowJo v10.0 software package.
Cell population abundance	n/a
Gating strategy	Examples and descriptions for all gating strategies are in the methods. For the two-cell (HER2+ and HER2-) assays, debris was gated out by the FSC and SSC area. For Siglec-Fc staining, (against a population of cells from a single cell line) cells were gated based on their size by FSC and SSC, followed by gating on single cells by linear gating on FSC-A and FSC-H. For extracted mouse tumors that were resuspended, debris and dead cells were first gated out on a SSCA-high /V450-A (violet live/dead stain) - negative population, followed by normal gating on area FSC-A/SSC-A followed by single cell gating with FSC-A/FSC-H.

- Tick this box to confirm that a figure exemplifying the gating strategy is provided in the Supplementary Information.